Graphene-Like Monoelemental 2D Materials for Perovskite Solar Cells

Selengesuren Suragtkhuu, Suvdanchimeg Sunderiya, Purevlkham Myagmarsereejid, Solongo Purevdorj, Abdulaziz S. R. Bati, Bujinlkham Bold, Yu Lin Zhong, Sarangerel Davaasambuu, and Munkhbayar Batmunkh*

Perovskite solar cells (PSCs) have attracted a great deal of attention from the photovoltaic (PV) community because of their remarkable performance, low production cost, and high potential to be integrated into other optoelectronic applications. Despite their promise, the challenges associated with their operational stability have drawn increasing attention over the past decade. Owing to their unique structure and fascinating properties such as high charge mobility, excellent conductivity, tunable bandgap, good optical transparency, and optimal surface functionalization, nanostructured materials, in particular monoelemental 2D materials, have recently been demonstrated to play versatile functions in suppressing the degradation of PSCs and enhancing the PV performance of the devices. In this review, recent advances in perovskite solar cells employing monoelemental 2D materials are presented. A brief overview of perovskite light absorbers based PV devices is first introduced, followed by critical discussions on the use of various elemental 2D materials including graphene, phosphorene, antimonene, borophene, bismuthene, and their derivatives for different components of the perovskite solar cells. Finally, the challenges in this cutting-edge research area are highlighted, and the authors express their own perspectives on addressing these key issues.

1. Introduction

With the rising energy costs and challenges over greenhouse gas emissions and climate change,[1] the world has witnessed an exponential increase in efforts over the past several years toward the energy transition from fossil fuel to clean energy. According to International Energy Agency (IEA), no investment in new fossil fuel supply projects will be made from today, while there will be no sales of new internal combustion engine passenger cars by 2035.[2] Renewable energy sources such as wind and solar energy are capable of generating around 70% of global electricity demand by 2050.[2] Solar photovoltaic (PV) technologies are of particular interest because the sun is the world's largest source of energy supply.

Impressively, solar cells made of silicon (Si) semiconductors provide a combination of excellent PV performance and a long lifetime. Their commercial modules can last for more than 20 years, and therefore, mono- and poly-crystalline Si solar cells make up >90% of the PV market.[3] Notably, recent progress in PV sector has led to a considerable reduction in the module price of Si solar cells, but the overall systems still suffer from high installation costs (known as balance of system) which are accountable for 75% of the system cost.[4] Therefore, further developments are still in demand in order to maximize

S. Suragtkhuu, P. Myagmarsereejid, Y. L. Zhong, M. Batmunkh
Queensland Micro- and Nanotechnology Centre
School of Environment and Science
Griffith University
Nathan, Queensland 4111, Australia
E-mail: m.batmunkh@griffith.edu.au
S. Sunderiya, S. Purevdorj, S. Davaasambuu
Department of Chemistry
Division of Natural Sciences
School of Arts and Sciences
National University of Mongolia
Ulaanbaatar 14200, Mongolia

A. S. R. Bati
Centre for Organic Photonics and Electronics (COPE)
School of Chemistry and Molecular Biosciences
The University of Queensland
Brisbane, Queensland 4072, Australia
B. Bold
Nano International LLC
UNIQ Center
Ikh Mongol Street, 15th Khoroo, Khan-Uul District,
Ulaanbaatar 17029, Mongolia
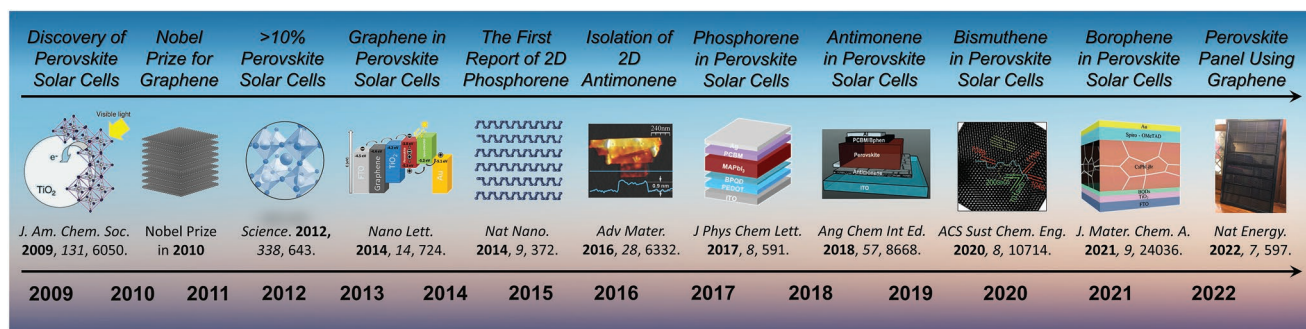
Figure 1. A timeline of the key achievements in the development of PSC, monoelemental 2D materials and their integrations. Reproduced with permission.[10a,12,13d,14–15] Copyright 2009, American Chemical Society.[10a] Copyright 2013, American Chemical Society.[14] Copyright 2016, Wiley-VCH.[15a] Copyright 2017, American Chemical Society.[15b] Copyright 2018, Wiley-VCH.[15c] Copyright 2020, American Chemical Society.[15d] Copyright 2021, Royal Society of Chemistry.[13d] Copyright 2022, Springer Nature Limited.[12]

the effectiveness of PV systems and reduce their fabrication cost. The key strategies include i) lowering the production cost of the system dramatically,[5] ii) developing tandem solar cells to improve the PV cell efficiency,[6] and iii) discovering new types of PV systems that can be at least comparable to a mature Si technology in terms of performances and lifetime while promising a low-cost.[7] Organic–inorganic halide perovskite structures-based solar cells have shown great promises for the requirements of all these strategies.[8]

Among a wide range of emerging classes of solar energy technology, perovskite solar cells (PSCs) are the most promising candidates to replace and/or to be integrated with Si solar cells. PSCs are a class of thin-film PV and constructed with a layered structure involving perovskite as a light-harvesting material. Besides the manufacturing process of PSCs is much easier than that of Si solar cells, their calculated cost was around 2 times cheaper than the Si systems.[9] The efficiencies of PSCs have increased faster than any other PV technologies in history, from 3.8% in 2009 to 25.7% in 2022,[10] making them the most advancing PV system. Notably, owing to their high efficiencies, perovskite-Si tandem solar cells very recently surpassed the milestone of 30% efficiency.[10b] Expectations are high in further improving PV efficiencies of both single-junction PSCs and perovskite-Si tandem solar cells. To be commercially viable, perovskite-based PV systems need to be scaled-up while maintaining excellent stabilities.

2D layered materials have shown specific promises in not only improving both efficiency and stability of PSCs,[11] but also the use of 2D materials has recently enabled the manufacturing of large-area (0.50 m²) perovskite solar panels.[12] In particular, monoelemental 2D layered materials such as graphene, phosphorene, borophene, antimonene, and others have gained much attention in PSC research due to their attractive properties including tunable bandgap, high charge carrier mobility, excellent conductivity, and high tunability in their surface structures.[13] Since the first report of graphene in PSCs in early-2014,[14] excellent progress has been made in employing graphene and other elemental 2D materials within the short period of time to solve some of the obstacles that hinder further development of PSCs.

Herein, we outline the advancements in high efficiency and stable PSCs realized using monoelemental 2D materials

including graphene, phosphorene, antimonene, borophene, and bismuthene. **Figure 1** displays the key progress in the development of PSCs and monoelemental 2D materials. We begin by providing a brief overview of PSCs. Then, the successful applications of various elemental 2D materials in different components (layers) of PSCs are presented. The review concludes by highlighting the key achievements in this rapidly growing research area and discussing the challenges requiring attention.

2. Overview of PSCs

Over the past decade, advances in designing and optimizing PSCs device architecture have been achieved with the aim of not only enhancing the extraction and transportation processes of photogenerated charge carriers, but also protecting the perovskite layer from the factors that affect its long-term operational stability such as moisture penetration, elevated temperature, and light soaking effect. In general, PSCs are assembled based on two main device configurations known as conventional (n-i-p) and inverted (p-i-n) structures (see **Figure 2**a for n-i-p and 2b for p-i-n). The main difference between these architectures is associated with the position of the charge transporting layer (CTL). In a conventional structure, the incident light initially passes through the electron transporting layer (ETL) before being absorbed by the perovskite layer, while the hole transporting layer (HTL) is employed as the rear CTL to collect photogenerated holes. On the contrary, the inverted PSCs are fabricated by utilizing the HTL and ETL as the front and rear CTL, respectively. A primary advantage of the devices with conventional configuration is their high efficiencies, while the inverted devices are much easier to fabricate and can deliver
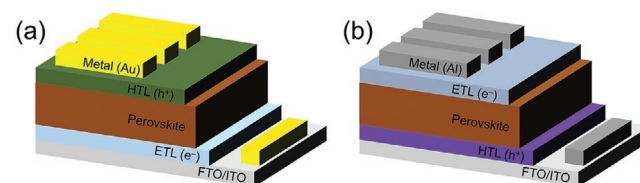
Figure 2. a) Conventional (n-i-p) and b) inverted (p-i-n) PSC devices.

**ADVANCED
SCIENCE NEWS**
www.advancedsciencenews.com

**ADVANCED
ENERGY
MATERIALS**
www.advenergymat.de

excellent PV performances. Promisingly, recent studies have shown that both n-i-p and p-i-n PSCs can achieve a negligible *J–V* hysteresis and can be fabricated using low-temperature processing materials.[16]

The basic operational mechanism of PSCs is independent of the device structure and can be briefly described as follows: 1) the incident photons are absorbed by the perovskite active layer generating excitons (electron-hole pairs); 2) CTLs on both perovskite sides aid in fast exciton dissociation and carrier transportations to the conductive electrodes (e.g., FTO/ITO or metal); 3) the flow of the collected charge carriers generates the electric current. Efficient charge extraction by both CTLs plays important roles not only in achieving high efficiency but also promoting perovskite crystal growth, suppressing ion migration, and reducing hysteresis. Therefore, the selection of robust and inexpensive ETL and HTL materials with high conductivity and mobility and suitable energy levels at the perovskite interfaces to efficiently transport electrons and holes is crucial for the realization of high efficiency and stable devices. To date, the majority of the state-of-the-art conventional n-i-p PSCs are constructed using titanium dioxide (TiO_2) or tin oxide (SnO_2) as the electron transporting material (ETM), while 2,2,7,7-tetrakis(*N,N*-pdimethoxyphenylamino)-9,9-spirobi-fluorene (Spiro-OMeTAD) is the typical material used as the hole transporting material (HTM).[8a] It is worth mentioning that the issues associated with device hysteresis and high processing temperature required for TiO_2 (>450 °C) represents the major drawbacks toward scalability and roll-to-roll fabrication on flexible substrates.[17] On the other hand, fullerenes and their derivatives such as 6,6-phenylC61butyric acid methyl ester (PCBM)) and poly(3,4 ethylenedioxythiophene)–polystyrene sulfonate (PEDOT:PSS) are known as excellent ETM and HTM in p-i-n PSCs, respectively.[18] Despite their widespread use, many of these materials used in CTLs suffer from several intrinsic drawbacks such as the poor conductivity and high grain-boundary density for TiO_2, the low hole mobility for pristine spiro-OMeTAD, and high acidic nature and low work function for PEDOT:PSS.[19] Great efforts have been made to address these challenges in PSC research. For example, doping Spiro-OMeTAD with lithium bis(trifluoromethylsulfonyl)imide (TFSI) has been found to increase its hole mobility by an order of magnitude;[20] however, the hygroscopic nature of lithium salts and lithium-ion migration inevitably degrade the device stability. In recent years, great advances have been accomplished in developing various ETMs and HTMs that have been proven to be competitive alternatives to fully replace the commonly used candidates.[21]

The development of novel materials with appealing chemical, physical, electronic, and optical properties is a promising path to overcome these shortcomings of PSCs. Of particular interest in this review is monoelemental 2D materials which have been intensively explored and drawn great recognition over the past few years.[22] The attractive features of these exciting materials include unique molecular structures and excellent fundamental properties such as high carrier mobility, layer, or structure dependent bandgap. In addition, the synthetic routes to produce these 2D materials include solution-processable and inexpensive approaches which have been proven to be promising for large-scale device fabrication using roll-to-roll technologies.

3. PSCs Using Monoelemental 2D Materials

Recently, elemental 2D materials have attracted growing attention since they offer important advantages such as low production cost, high degree of tunable properties and structure tailoring, and excellent compatibility with solution processing. Notably, since the discovery of graphene as the first monoelemental 2D material in 2004,[23] exciting advancements have been made in graphene research and resulted in the Nobel Prize in Physics in 2010. Moreover, impressive progresses have been made in PSC research over the past more than a decade. A broad spectrum of 2D nanomaterials such as graphene derivatives, metal carbides/nitrides (MXene), transition metal dichalcogenides (TMDs), and elemental 2D materials have been employed in PSCs.[13a,24] Generally, 2D materials consist of a monolayer or few-layers nanosheets, bonded with weak out-of-plane van der Waals bond, and strong unique in-plane chemical bonds, resulting their chemical and physical properties more extraordinary.[25] For instance, graphene with hexagonal honeycomb lattice formed by sp^2 hybridization making it a highly conductive material.[23] On the other hand, 2D materials with buckled honeycomb structured sp^2/sp^3 could act as semiconductors with high carrier mobility and tunable bandgap to match in PSCs.[26] **Table 1** summarizes the key fundamental properties of the widely explored 2D materials in comparison to monoelemental 2D materials. It can be clearly seen from Table 1 that the major challenge in monoelemental 2D materials is their stability in an aqueous solvent and ambient conditions although they show very defined and controllable electronic properties.

Indeed, the first use of graphene in PSCs was reported in 2014,[14] while phosphorene was discovered and introduced as a new member to the monoelemental 2D family in 2014.[38] More importantly, we have witnessed a significant step forward in the emergence of monoelemental 2D materials for PSCs. A wide range of 2D materials including graphene, phosphorene, antimonene, borophene, bismuthene, and their functionalized forms have been employed in PSCs. While these 2D materials show many promising properties, their suitable and tunable energy band alignments are of particular importance for use in PV applications. **Figure 3** depicts the energy level diagram of the commonly used materials for CTL, front electrode, perovskite light absorbers and monoelemental 2D materials for PSCs. The following sections will discuss the exciting advances that have been made in using various monoelemental 2D materials in different components of PSCs.

3.1. Transparent Conductive Electrode (TCE)

A TCE is an essential component of PSCs. The optical transparency of the TCE defines the amount of light passing into the photoactive perovskite layer, while its electrical conductivity ensures the rapid transportation of photogenerated charges to the external circuit.[40] In general, high efficiency PSCs rely strongly on the use of indium-doped tin oxide (ITO), fluorine-doped tin oxide (FTO), and indium-doped zinc oxide (IZO) as the TCEs owing to their high optical transparencies and low sheet resistance.[41] Despite having these excellent properties,

Table 1. Overview of fundamental properties of various 2D materials.

2D material	Bandgap [eV]	Carrier mobility [cm^2 V^{-1} s^{-1}]	Stability in water	Stability in air	Refs.
Graphene	0	≈2×10^5	Very stable	Very stable	[11a,27]
Graphene oxide	0.11–3.00	≈0.05–10	Very stable	Very stable	[28]
Reduced graphene oxide	0.02–3.00	≈2–200	Very stable	Stable	[29]
Phosphorene	0.3–2.0	≈1000	Very unstable	Very unstable	[11a,27,30]
Antimonene	0–2.28	0.5–1.2×10^3	Very unstable	Very unstable	[31]
Borophene	0.20–1.30	≈1.51×10^3	Unstable	Unstable	[32]
Bismuthene	0.99	322.3	Stable	Stable	[31a,c,33]
MXene (Ti$_3$C$_2$T$_x$)	0–3.4	≈34	Unstable	Unstable	[24a,34]
TMDs (MoS$_2$)	1.2–1.8	10–200	Stable	Stable	[35]
TMDs (WS$_2$)	1.3–2.1	43–234	Stable	Stable	[36]
TMDs (TiS$_2$)	0.02–2.5	7.24	Stable	Stable	[37]

traditional TCEs suffer from several drawbacks including the limited resources of the raw product (e.g., indium), poor flexibility and high structural defects.[42] These issues have led to excellent efforts being focused on the replacement of conventional TCEs with cheaper alternatives such as carbon materials, 2D materials, conductive polymers, metal-based nanostructures, and others.[43] In terms of monoelemental 2D materials, unlike graphene, the majority of these 2D materials exhibit excellent semiconducting properties owing to their tunable bandgaps. Considering the requirement of high electrical conductivity for ideal TCEs, we expect that the semiconducting nature of the most monoelemental 2D materials (e.g., phosphorene, antimonene) would limit the practical utilization of these materials as TCEs. However, interface engineering using these 2D materials would be a valuable strategy to suppress the charge recombination in solar cells. **Table 2** presents the PV parameters of PSCs constructed using 2D materials-based TCEs.

On the other hand, graphene has been proven to be a promising candidate as a TCE material due to their natural abundance, low-cost, mechanical flexibility, and excellent stability.[47] To the best of our knowledge, in 2015, Sung et al.[44] reported for the first time the use of graphene as a TCE for PSCs. An inverted PSC with a layered structure of graphene/MoO$_3$/PEDOT:PSS/MAPbI$_3$/C$_{60}$/bathocuproine (BCP)/LiF/Al was constructed (**Figure 4**a), where a few nanometer thick MoO$_3$

layer played a critical role by providing excellent hydrophilicity to the graphene surface and adjusting the work function of the electrodes. With the optimum MoO$_3$ thickness of 2 nm, graphene TCE based PSC delivered a power conversion efficiency (PCE) of 17.1%, which was not too far from that (18.8%) of the device assembled on a conventional ITO electrode. It should be noted that the sheet resistance of the graphene film on a glass substrate before and after depositing MoO$_3$ (2 nm) was measured to be >2 and 0.5 kΩ cm^{-2}, respectively, demonstrating the significance of MoO$_3$ layer in this graphene based inverted (p-i-n) PSC. In this pioneering work by Sung et al.,[44] graphene was grown using a chemical vapor deposition (CVD) method. Although CVD-grown graphene provides less structural defects and high electrical conductivity, solution processable graphene structures are appealing because of their applicability on large-area flexible substrates and is compatibility with roll-to-roll manufacturing routes. Indeed, Batmunkh et al.[45] was the first to develop solution processed graphene TCEs to replace the traditional FTO electrode in n-i-p PSCs. In this work, the authors fabricated transparent films with different thicknesses from chemically and thermally derived graphene and used them as the TCE in CH$_3$NH$_3$PbI$_{3-x}$Cl$_x$ perovskite based solar cells (Figure 4b). By using the electrode with an optimized graphene thickness, a PCE of only 0.62% was achieved. The main PV parameters responsible for this low cell efficiency were the poor current density (J_{sc}) and fill factor (FF) values, which can
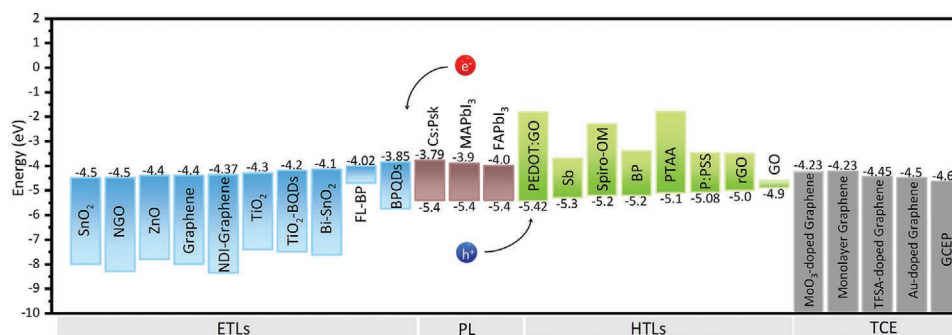
Figure 3. Energy level diagram of the commonly used materials and monoelemental 2D materials for PSCs. The values of the energy levels were collected from literature.[11a,13d,15d,39]

Table 2. PV parameters of PSCs fabricated with monoelemental 2D materials-based transparent electrodes and their corresponding device stability and bending tests. Note: the aging and bending test results are presented only for the devices with 2D materials.

Device structure	J_{sc}; [mA cm^{-2}]	V_{oc}; [V]	FF	PCE; [%]	Retained %/aging time/condition	Retained %/bending cycle/radius	Refs.
Glass/graphene/MoO$_3$/PEDOT:PSS/CH$_3$NH$_3$PbI$_3$/C$_{60}$/BCP/LIF/Al;	21.50	1.06	0.75	17.1	–	–	[44]
Glass/AuNPs-rGO/cp-TiO$_2$/mp-TiO$_2$/CH$_3$NH$_3$PbI$_{3-x}$Cl$_x$/Spiro-OMeTAD/Au;	2.55	0.69	0.35	0.62	–	–	[45]
PEN/graphene/MoO$_3$/PEDOT:PSS/CH$_3$NH$_3$PbI$_3$/C60/BCP/LiF/Al;	21.70	1.00	0.78	16.8	–	85%/5000 cycle/2 mm	[39m]
Glass/TFSA-doped graphene/PEDOT: PSS/FAPbI$_{3-x}$Br$_x$/PCBM/Al;	21.45	1.07	0.77	18.2	95%/1000 h/1 Sun at 60 °C and 30% RH	35%/5000 cycle/4 mm	[39p]
Glass/AuCl$_3$-doped graphene/PEDOT: PSS/CH$_3$NH$_3$PbI$_3$/PCBM/Al;	21.00	1.09	0.78	17.9	>95%/100 h/1 Sun at 50% RH	–	[46]
PES/graphene/NiO$_x$/CH$_3$NH$_3$PbI$_3$/PCBM/AZO/Ag/AZO;	20.90	0.93	0.73	14.2	–	91%/1000 cycle/strain @ 1.5%	[39n]
PI/Cu-grid/graphene/PEDOT:PSS/perovskite/PC$_{61}$BM/ZnO/Ag;	21.70	0.99	0.76	16.4	–	97%/10 000 cycle/5 mm	[39r]

be elucidated by the high sheet resistance (3.08 kΩ sq^{-1}) at low optical transparency (55% at a wavelength of 550 nm). Although this work demonstrates the feasibility of solution processed graphene based TCEs in PSC devices, future studies should aim to minimize the sheet resistance of the transparent films. Novel electrode designs using solution processable graphene and conductive metal structures would be a promising route to achieve high performance TCEs.

It is well documented that graphene shows outstanding mechanical robustness, making it attractive for flexible devices. In 2016, Yoon et al.[39m] made an effort to demonstrate efficient PSCs with high flexibility using MoO$_3$-deposited CVD-grown graphene on polyethylene naphthalate (PEN) substrates

(Gr-Mo/PEN). The fabricated flexible p-i-n PSCs using graphene TCEs reached an efficiency of 16.8% with no hysteresis, while the flexible ITO electrode based device showed a PCE of 17.3%. Importantly, the Gr-MoO$_3$/PEN device showed an outstanding bending stability after 1000 repeated cycles at a bending radius of 4 mm (R = 4 mm), whereas the PCE of the ITO/PEN based device decreased to 80%, 60%, and 25% of its initial value after 500, 750, and 1000 bending cycles, respectively (Figure 4d,e). This superior robustness against mechanical deformation of graphene TCEs based flexible PSCs shows great promise for the development of foldable PV devices. This innovative research has inspired researchers to further develop high efficiency and super-flexibility PSCs. A PCE of 18.3% was
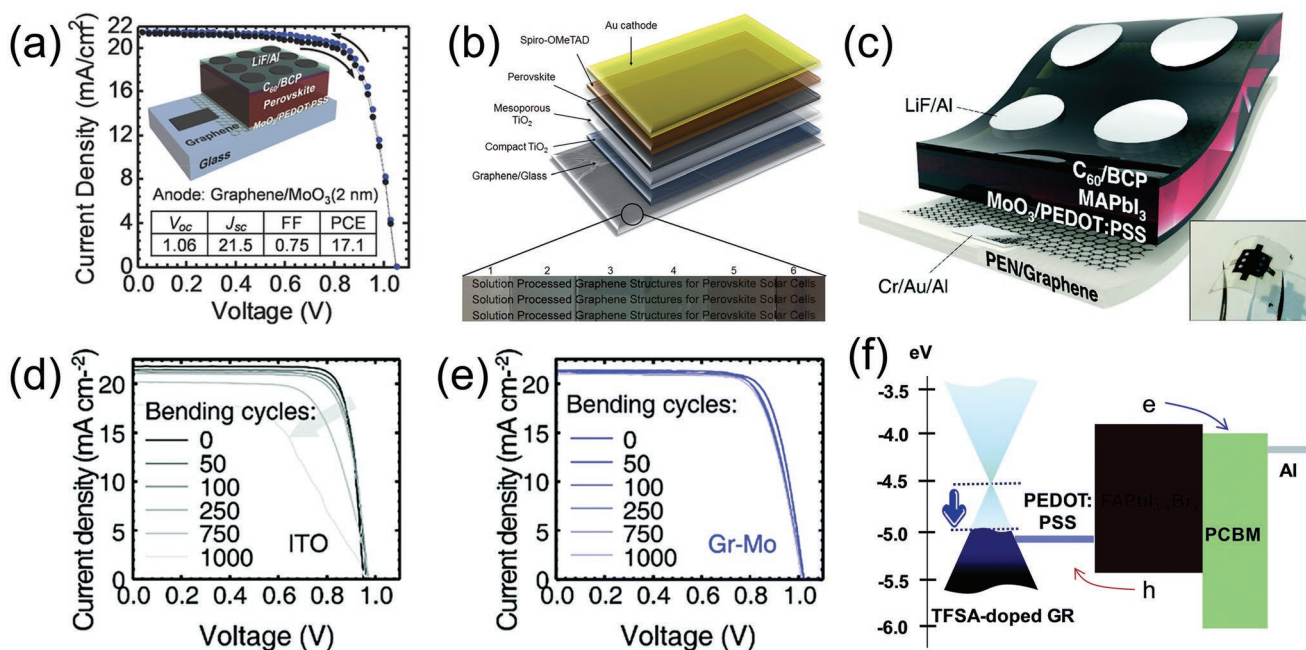
Figure 4. a) J–V curve of inverted PSC constructed using graphene as a TCE. Inset shows the corresponding device architecture.[44] Reproduced with permission.[44] Copyright 2016, Wiley-VCH. b) Schematic illustration of a PSC structure employing transparent electrodes made from solution processed graphene.[45] Reproduced with permission.[45] Copyright 2016, Royal Society of Chemistry. c) Device structure of graphene-based flexible PSC. Inset shows the photograph of a complete cell. J–V curves of the d) ITO/PEN and e) Gr-Mo/PEN based PSCs during bending of up to 1000 cycles at R = 4 mm.[39m] Reproduced with permission.[39m] Copyright 2017, Royal Society of Chemistry. f) Energy band diagram of TFSA-doped graphene electrode based p-i-n PSC.[39p] Reproduced with permission.[39p] Copyright 2018, Royal Society of Chemistry.

**ADVANCED
SCIENCE NEWS**

www.advancedsciencenews.com

**ADVANCED
ENERGY
MATERIALS**

www.advenergymat.de

achieved $FAPbI_{3-x}Br_x$ perovskite based flexible device (p-i-n) using a bis(trifluoromethanesulfonyl)-amide (TFSA)-doped CVD-grown graphene electrode.[39p] The photostability of this TFSA-doped graphene electrode based device was tested under a continuous light (1 Sun) soaking at 60 °C/30% relative humidity for 1000 h. Remarkably, the device retained 94.7% of its initial performance, while displaying excellent bending stabilities over 5000 bending cycles. This work demonstrates that doping strategies not only enhance the electrical conductivities, but also effectively tune the energy band alignment of the electrodes. A simple $AuCl_3$ was also found to be an effective dopant which can increase the work function of graphene from 4.52 to 4.86 eV, while also decreasing the sheet resistance from 890 to 70 Ω cm^{-2}, leading to remarkable enhancements in the efficiencies.[46] Since chemical doping is a powerful method to adjust the work function and increase the conductivity of graphene electrodes, attempts should be made using other types of doping agents to reveal the best dopant for graphene TCEs-based PSCs.

An interesting study was conducted by Tran et al.,[39n] who employed plasma-assisted thermal CVD method to prepare monolayer graphene a polymer substrate at low temperature (150 °C). The prepared graphene electrode was used to construct flexible PSCs with a layered architecture of polyester-sulfone (PES)/graphene/NiO_x/$MAPbI_3$/PCBM/AZO-Ag-AZO. For comparison, the control device was also fabricated on CVD-grown graphene electrode prepared using a high temperature (950 °C). Raman results revealed that defect-free and single crystalline graphene was achieved for using the PATCVD method. The sheet resistance of PATCVD based graphene displayed a sheet resistance of 82 Ω cm^{-2} which was significantly lower than that of the control graphene (2080 Ω cm^{-2}). The PCE of PATCVD-Gr device was measured to be 14.18%, while the control device fabricated using the CVD-graphene showed a PCE of only 11.65%. More importantly, the fabricated flexible solar cells presented excellent stabilities after 1000 cycles of curvature at $R = 4$ mm, retaining 95% of its initial PCE. Further modification and functionalization of PATCVD-based graphene electrodes would be valuable strategy for realizing high efficiency flexible and semitransparent PSCs.

Utilizing metallic structures such as wires and meshes has been attractive way to achieve high performance TCEs due to their excellent electrical conductivities.[48] However, the metal-based transparent electrodes themselves suffer from issues associated with the stabilities due to the interdiffusion of metals and halide ions. In a recent study, Jeong et al.[39r] demonstrated that flexible hybrid TCEs made of a Cu grid-embedded polyimide film and graphene layer displays excellent mechanical and chemical stabilities. The role of graphene in this TCE was to prevent metal-induced degradation and halide diffusion between the perovskite layer and electrode. Moreover, the graphene layer provided an extra charge conducting pathways, reducing the sheet resistance of the electrode to 5.2 Ω sq^{-1}. A PCE of 16.4% was achieved using this novel TCE based flexible PSC, whereas the reference cells with ITO on glass and PET substrate exhibited PCE values of 17.5% and 15.1%, respectively. The authors also demonstrated that their flexible device employing Cu grid-embedded polyamide and graphene can withstand under up to 10 000 bending cycles at a radius of 5 mm. Since this study provides useful ways to overcome the issues of metal-induced degradation when using metal-based TCEs, future work should focus on employing other types, structures and designs of metals integrated with highly conductive graphene. Moreover, the development of flexible PSCs with high optical transparencies would be of great value for integrating the novel devices into other advanced applications such as building integrated PV (BIPVs).

3.2. Electron Transporting Layer (ETL)

For high efficiency PSC devices, ETL plays a vital role not only in extracting and transporting the charge carriers, but also for the device stability and scalability.[49] In order to achieve high performance PSCs, an ideal ETL should efficiently extract the photogenerated electrons from the perovskite layer and transport them to the conductive electrode, while suppressing the nonradiative recombination.[21b,50] Metal oxides such us titanium oxide (TiO_2), tin oxide (SnO_2), and zinc oxide (ZnO) are the most commonly fabricated as ETL in n-i-p device configuration, while fullerene and PCBM are typically employed in inverted PSCs because of their favorable properties such as good chemical stability, suitable energy level, and intriguing optoelectronic properties.[21b,50–51] Despite these promising properties, further improvements in their electron mobility and stability under UV-light exposure are still required for the fabrication of high efficiency and stable PSCs. In this regard, graphene-like 2D materials hold specific promise in improving the ETLs of high efficiency PSCs.

Integrating graphene and its derivatives into the ETL has been proven effective strategy to enhance the efficiency of different solar cells, before even being applied in PSCs.[52] In most cases, graphene-based materials are used to improve the charge transporting properties of the devices due to their high conductivity. Indeed, the first study on using graphene in the ETL of PSCs was reported by Wang et al.[14] who employed graphene to prepare low-temperature processed ETL. Notably, the low-temperature processing is appealing for PV technology as it opens opportunities for designing flexible devices. The authors were able to fabricate PSCs using nanocomposites of graphene and TiO_2 nanoparticles as the ETL at temperatures no higher than 150 °C. Owing to the superior charge-collection of TiO_2-graphene nanocomposites and suitable energy alignment (**Figure 5**a), the fabricated devices showed a PCE of up to 15.6%, while the PSC assembled using low-temperature processed TiO_2-only ETL displayed an efficiency of only 10%. Considering the processibility, the low-temperature processed TiO_2-graphene nanocomposite based ETLs could be compatible with roll-to-roll manufacturing technique, meeting the needs of large scale industrial fabrications. Furthermore, Han and colleagues added reduced graphene oxide (rGO) to the mesoporous TiO_2 (mp-TiO_2) based ETLs (high-temperature processed) to improve the charge collection efficiency of n-i-p PSCs.[53] The observed enhancement in the efficiency by using rGO was 18%. Batmunkh et al.[45] also demonstrated the same concept, but the devices were fabricated on graphene-based TCEs.

Unlike graphene and rGO nanosheets, graphene oxide (GO) shows poor electrical conductivity. Interestingly, in 2016,
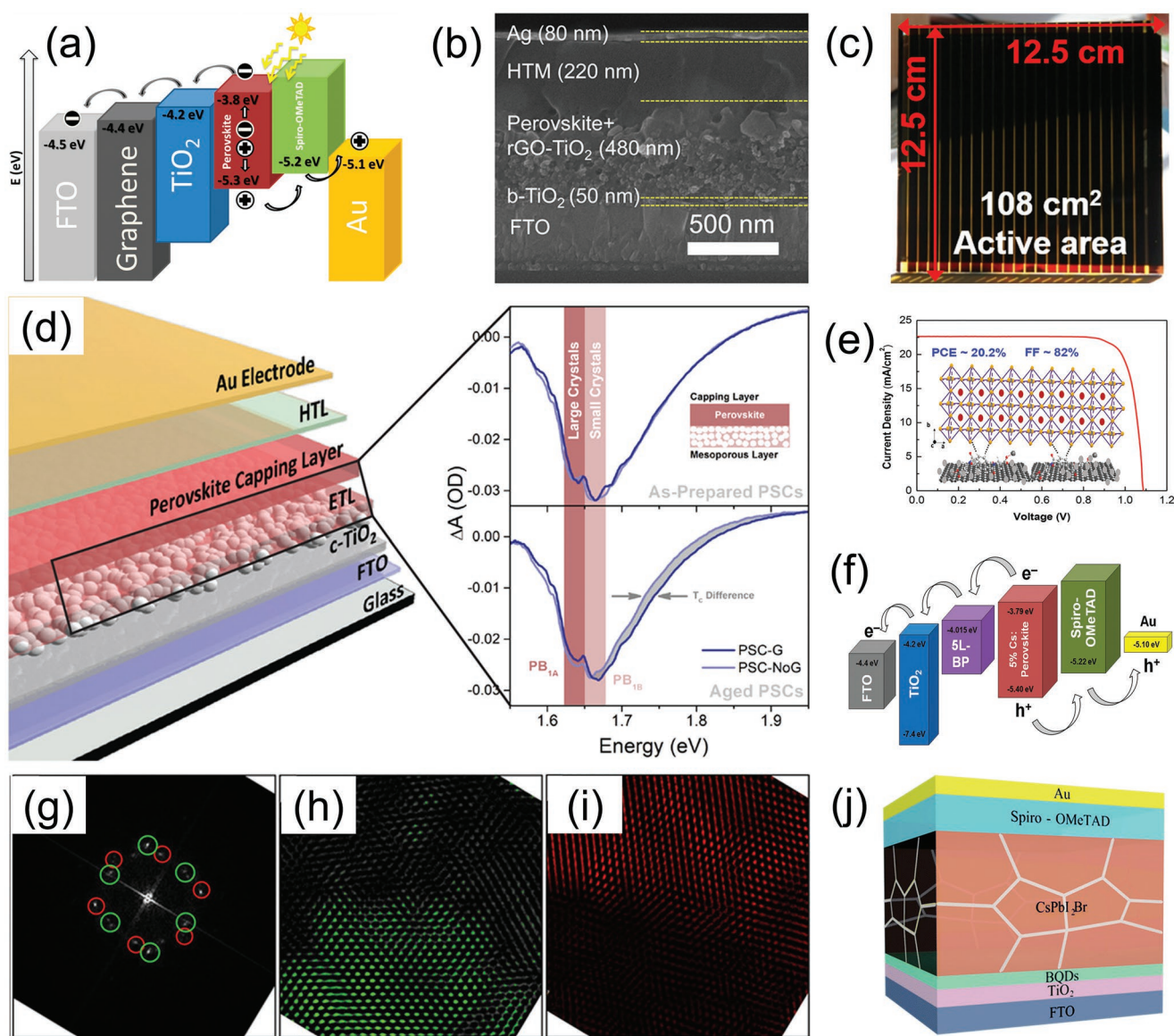
Figure 5. a) Schematic illustration of energy band alignment of TiO$_2$-graphene nanocomposite-based PSC.[14] Reproduced with permission.[14] Copyright 2014, American Chemical Society. b) Cross-sectional scanning electron microscopy (SEM) image of PSC employing rGO added mp-TiO$_2$ based ETL. Reproduced with permission.[53] Copyright 2015, American Chemical Society. c) Photograph of a perovskite PV module (108 cm^2 active area, 156.25 cm^2 substrate area).[55a] Reproduced with permission.[55a] Copyright 2015, American Chemical Society. d) Schematic illustration of the layered structure of PSC fabricated with graphene inserted mp-TiO$_2$. The corresponding transient absorption spectra acquired at pump–probe time delay of 0.75 ps for the as-prepared and aged PSCs with and without graphene.[56] Reproduced with permission.[56] Copyright 2019, American Chemical Society. e) J–V curve of NDI-graphene added SnO$_2$ ETL based PSC. Inset shows the chemical structure of NDI and the bonding condition of NDI-graphene with perovskite films.[39c] Reproduced with permission.[39c] Copyright 2018, American Chemical Society. f) Energy level alignment of five-layer BP incorporated TiO$_2$ ETL-based n-i-p PSC. Reproduced with permission.[39d] Copyright 2019, Wiley-VCH. g) Fast Fourier transform (FFT) image of bismuthene-SnO$_2$ (Bi-SnO$_2$), highlighting the h) SnO$_2$ lattice (green) and i) Bi lattice (red).[15d] Reproduced with permission.[15d] Copyright 2020, American Chemical Society. j) Layered structure of a PSC fabricated using borophene quantum dots as a surface passivation agent on the TiO$_2$ layer.[13d] Reproduced with permission.[13d] Copyright 2021, Royal Society of Chemistry.

Carlo's group used GO, after neutralizing with lithium (Li), as the ETL on top of mp-TiO$_2$ for PSCs, where Li neutralization helps to modify the work function of the ETL.[54] Owing to the good energy matching with the TiO$_2$ conduction band, GO-Li inserted PSCs showed improved PV efficiency from 10.3% to 11.8%. Importantly, the authors showed that the insertion of GO-Li between the mp-TiO$_2$ and perovskite layers

improves the hysteresis and stability of the devices. Since their first work on using GO-Li in the ETL of PSCs,[54] the same group of researchers led by Bonaccorso and Carlo incorporated graphene-based structures in different layers of PSCs including the ETLs to fabricate large area modules and also perovskite/silicon tandem solar cells.[55] For example, a module with an active area of 108 cm^2, delivering 13.4% efficiency, was

**ADVANCED
SCIENCE NEWS**

www.advancedsciencenews.com

**ADVANCED
ENERGY
MATERIALS**

www.advenergymat.de

fabricated by integrating graphene structures in both compact TiO_2 (cp-TiO_2) and mesoporous TiO_2 (mp-TiO_2) layers, while also inserting MoS_2 layer between the perovskite and HTL.[55a] These works demonstrate that 2D materials have the potential to play roles in the commercialization of PSCs. Despite the promises, the stability of PSCs still remains an issue that calls for a solution. Interestingly, Carlo and colleagues showed that the incorporation of graphene flakes in the mesoporous TiO_2 leads to stable values of carrier temperature.[56] The carrier temperature of PSCs fabricated without graphene decreased by about 500 K over 1 week, while the graphene incorporated device showed a reduction of less than 200 K after the same aging time. Moreover, the authors showed using femtosecond transient absorption measurements that the use of graphene is beneficial for constructing stable PSCs (Figure 5d). Although excellent progress has been made in employing 2D graphene in TiO_2-based ETLs, other oxide semiconductors have become more promising ETMs for PSCs.

Besides TiO_2, ETLs made from SnO_2 have attracted much attention owing to their wide bandgap, excellent chemical stability, high carrier mobility, and simplified device configuration, while also requiring lower annealing temperature (<180 °C) than TiO_2 (>450 °C).[57] However, one of the main bottlenecks in SnO_2-based ETLs is their significant trap states, resulting in limited PV performance and serious hysteresis. In 2017, Xie et al.[58] used graphene quantum dots to improve the electronic properties of SnO_2 ETL for PSCs. They found that the graphene quantum dots not only fill the electron traps, but also enhance the conductivity of SnO_2, and thus reducing the charge recombination at the interface of ETL and perovskite. A PCE of 20.31% with very little hysteresis was achieved, while the control device without graphene showed an efficiency of 17.91%. In particular, the FF values of their devices without and with graphene quantum dots were 0.74 and 0.78, respectively. It should be noted that SnO_2 ETL based PSCs often deliver high FF values, but Wang's group aimed to further boost the FF >0.80 using surfactant (N,N'-bis-[2-(ethanoic acid sodium)]-1,4,5,8-naphthalene diimide (NDI)) modified graphene (NDI-graphene) in the SnO_2 layer.[39c] The role of NDI was to improve the dispersibility of exfoliated graphene in an aqueous solution while also tuning the energy level of graphene. As a result, an impressive FF value of 0.82 was achieved, yielding a PCE of 20.16%, using the NDI-graphene incorporated SnO_2 based solar cells. Another crucial factor to achieve highly efficient PSCs using SnO_2 is to control the oxygen vacancies. The optical and electrical properties of SnO_2 are controlled by oxidation state of Sn.[16a] Consequently, nitrogen-doped graphene oxide (NGO) was applied as an oxidizing agent for Sn^{2+} in SnO_2, while passivating the oxygen vacancies of the ETL.[39a] This newly introduced composite ETL resulted in improved values of V_{oc} (1.14 V) and FF (0.68) as compared to the control device without NGO. It can be clearly seen based on these studies that considerable level of efforts have been made in using graphene derivatives and their functionalized forms in the ETL of PSCs. However, research progress on the development of other monoelemental 2D materials based PSCs was relatively scarce despite the great advancements in the discovery of new members to the 2D family.

Unlike graphene, the majority of monoelemental 2D materials such as phosphorene, antimonene, and bismuthene show excellent semiconducting properties with tunable bandgaps, making them attractive for PV applications.[27,59] A single- or few-layer of black phosphorus (BP), known as phosphorene, has recently drawn increasing attention for PV devices owing to its high carrier mobility and tunable energy band alignment.[60] When 2D materials are used for ETL of solar cells, they are usually integrated with the conventional ETMs to observe improved efficiencies. Interestingly, because of their suitable energy alignment and promising electron selectivity, Fu et al.[39h] prepared and used BP quantum dots (BPQDs) as dual-functional electron selective layer to substitute traditional metal oxide-based ETLs in PSCs. In this class of devices, BPQDs provide suitable energy band alignment to facilitate the electron extraction from the perovskite ($FA_{0.85}MA_{0.15}PbI_{2.5}Br_{0.5}$) to the ETL. By using BPQDs as the only ETM, the authors achieved PCEs of 11.26% and 14.61% using the plastic and rigid substrates based PSCs, respectively. To demonstrate the effect of BPQDs as ETM, a control device without ETL was also fabricated. The ETL-free PSC displayed an efficiency of only 3.58%. This work paves the way for developing nonoxide materials-based ETLs for high efficiency PSCs. Chemical functionalization and/or doping strategies are greatly expected to modify the electronic properties of BP structures and will be of great value in realizing efficient PSCs.

Although it is reported that BP derivatives can be used themselves as ETMs, the fabrication of efficient PSCs is of great importance and can be achieved by incorporating them with other traditional oxide semiconductors. However, when integrating BP with TiO_2, particular attention should paid to the following two points: i) BP sublimes at a temperature of >300 °C, and ii) TiO_2 often requires annealing steps at high temperatures (>450 °C). Batmunkh et al.[39d] developed an efficient and easy route to prepare highly crystalline and atomically thin few-layer BP in isopropyl alcohol using a vortex fluidic device. The as-prepared few-layer BP was used as an effective ETM by integrating with low-temperature (<150 °C) processed TiO_2 for planar n-i-p PSCs. The device fabricated with phosphorene nanosheets showed a maximum efficiency of 17.85%, whereas the TiO_2-only ETL-based PSC displayed an efficiency of 16.35%. Their experimental and theoretical investigations revealed this efficiency enhancement was due to the suitable band alignment and high carrier mobility of the few-layer BP nanosheets (Figure 5f). As discussed earlier, a serious hysteresis effect observed during the reverse and forward scan is the main issue in PSCs fabricated using SnO_2 ETLs. Very recently, BPQDs were used as an additive to a precursor solution of SnO_2 nanoparticles for PSCs.[39e] Not only a high PCE of 21% was achieved, the SnO_2/BPQDs-based device showed an outstanding stability (1000 h under AM 1.5G lamp irradiation) and negligible hysteresis.

Besides graphene and phosphorene, efforts have shown that monoelemental borophene and bismuthene are promising candidates as ETMs of PSCs. Bismuthene with its small bandgap as compared to other typical semiconductors has been used in electronic applications,[61] but its appearance in PV devices has been very scarce. The only study incorporating 2D bismuthene in the ETL of PSCs that we are aware of was by Xue et al.,[15d] where SnO_2 nanoparticles and bismuthene sheets were coupled at a low-temperature based on a unique self-adaptive

feature of 2D bismuthene, in combination with the lattice-matching attribute of adjacent lattice-spacing between SnO_2 and bismuthene (see Figure 5g–i). Although no significant improvements were observed in the efficiency and hysteresis of PSCs by employing 2D bismuthene in the SnO2 ETL, the device constructed with Bi-SnO$_2$ ETL was able to store 80% of its initial PCE after aging over 800 h, whereas the control cell lost about 50% of its original value. The enhancement in the device stability was due mainly to the improved hydrophobicity of the ETL with bismuthene. On the other hand, borophene, mono-, or few-layer of boron, is an exciting 2D material having outstanding properties such as anisotropic metallic behavior and excellent flexibility.[62] Recently, borophene quantum dots were prepared using a sonication-assisted solution processable method and used as a surface passivation agent on the TiO_2-based ETL for inorganic (CsPbI$_2$Br) PSCs (Figure 5j).[13d] The authors observed strong interactions of boron atoms with both TiO_2 and perovskite, providing effective charge transport through the formation of a cascade energy alignment. As a result, borophene-based PSCs delivered a high PCE of 15.31%, which was higher than that (14.24%) of the device without borophene. Promisingly, the optimized PSCs with borophene exhibited excellent stability, maintaining 94% of its initial PCE after 40 days at a relative humidity (RH) of 20%. This work opens new research avenues for using 2D borophene for PV applications and other optoelectronic devices.

Furthermore, as an attractive member of 2D materials' family, antimonene has shown great promise in different types of solar cells.[24b,63] However, to the best of our knowledge, there has been no effort on using antimonene nanosheets for ETL of PV devices. This is likely to be due to the position of conduction band and p-type dominated electronic properties of antimonene.[63b] It can be observed from **Table 3** that there is a lack of effort in developing flexible PSCs (no bending tests were conducted) when 2D materials are used in ETLs. This would be important research to demonstrate the excellent mechanical properties of monoelemental 2D materials.

3.3. Perovskite Layer (PL)

In PSCs, the PL plays a critical role in absorbing lights and efficiently generating electron–hole pairs. The morphology, thickness, and grain size of the PL are important factors that show influences on the carrier mobilities, electronic properties, and performance of the devices.[64] Indeed the growth of PL with high crystallinity and low-defect is the key to the fabrication of high performance PSCs. Over the past several years, various types of preparation strategies have been developed to obtain high-quality perovskite films. One of the most effective strategies is the additive-assisted growth method.[65] In this regard, 2D materials are considered as promising additive materials in the PL of PSCs because of their excellent PV properties and tunable bandgaps. In 2016, Hadadian et al.[66] reported for the first time that the introduction of N-doped rGO (N-rGO) nanosheets (**Figure 6**a) improves the morphology of the PL while effectively passivating the surface at the perovskite/spiro interface. In particular, the use of N-rGO increased the perovskite grain size by slowing down the crystallization process, leading to high J_{sc} and FF values. In addition, the surface passivation of the perovskite by N-rGO sheets suppressed the charge recombination, and thus resulting in an improved V_{oc}. As a result, the device fabricated with N-rGO in the PL showed a PCE of 18.7% which was higher than that (17.3%) of the PSC without N-rGO.

Furthermore, Hahn's group significantly improved the stability of PSCs by integrating silver nanoparticle-anchored rGO (Ag-rGO) composites in the PL (CH$_3$NH$_3$PbI$_{3-x}$Cl$_x$).[67] They found that the addition of Ag-rGO in the PL not only suppresses the ion migration, but enhances the thermal and light stabilities of PSCs. The device fabricated with Ag-rGO incorporated PL was able to retain more than 94% of its initial PCE value after aging at a temperature 90 °C for 90 h, whereas the reference cell without additive sustained only around 60% of the initial performance. The result that was more exceptional in this work was the long-term stability of the devices with Ag-rGO, retaining nearly 100% of the initial PCEs after being

Table 3. PV parameters of PSCs fabricated with monoelemental 2D materials-based ETLs and their corresponding device stability and bending tests. Note: the aging and bending test results are presented only for the devices with 2D materials.

Device structure	J_{sc}; [mA cm^{-2}]	V_{oc}; [V]	FF	PCE; [%]	Retained %/aging time/ condition	Retained %/bending cycle/radius	Refs.
FTO/Graphene/TiO$_2$/CH$_3$NH$_3$PbI$_{3-x}$Cl$_x$/Spiro-OMeTAD/Au;	21.90	1.04	0.73	15.6	–	–	[14]
FTO/TiO$_2$-only/CH$_3$NH$_3$PbI$_{3-x}$Cl$_x$/Spiro-OMeTAD/Au;	17.70	1.00	0.61	10.0			
FTO/cp-TiO$_2$/rGO-mp-TiO$_2$/CH$_3$NH$_3$PbI$_3$/Spiro-OMeTAD/Au;	21.00	0.91	0.71	13.5	–	–	[53]
FTO/cp-TiO$_2$/mp-TiO$_2$/CH$_3$NH$_3$PbI$_3$/Spiro-OMeTAD/Au;	19.60	0.86	0.67	11.5			
ITO/SnO$_2$-GQDs/CH$_3$NH$_3$PbI$_3$/Spiro -OMeTAD/Au;	23.05	1.13	0.78	20.3	95%/90 days/at 30% RH	–	[58]
ITO/SnO$_2$/CH$_3$NH$_3$PbI$_3$/Spiro-OMeTAD/Au;	22.10	1.10	0.74	17.9			
ITO/SnO$_2$-NDI-graphene/perovskite/Spiro-OMeTAD/Au;	22.66	1.08	0.82	20.2	≈ 95%/300 h/at 30% RH	–	[39c]
ITO/SnO$_2$/perovskite/Spiro-OMeTAD/Au;	23.21	1.10	0.75	18.9			
PEN/ITO/BPQDs/perovskite/Spiro-OMeTAD/Au;	16.77	1.03	0.65	11.3	–	88.7%/200 cycles/5 mm	[39h]
FTO/TiO$_2$-phosphorene/perovskite/Spiro-OMeTAD/Au;	23.32	1.08	0.71	17.9	–	–	[39d]
FTO/TiO$_2$/perovskite/Spiro-OMeTAD/Au;	22.21	1.07	0.69	16.4			
FTO/bismuthene-SnO$_2$/perovskite/Spiro-OMeTAD/Au;	23.61	1.06	0.75	18.8	80%/800 h/at 5% RH	–	[15d]
FTO/SnO$_2$/perovskite/Spiro-OMeTAD/Au;	22.78	1.04	0.73	17.4			
FTO/TiO$_2$/borophene/CsPbI$_2$Br/Spiro-OMeTAD/Au;	15.18	1.28	0.79	15.3	94%/40 days/at 20% RH	–	[13d]
FTO/TiO$_2$/CsPbI$_2$Br/Spiro-OMeTAD/Au	15.14	1.24	0.76	14.2			
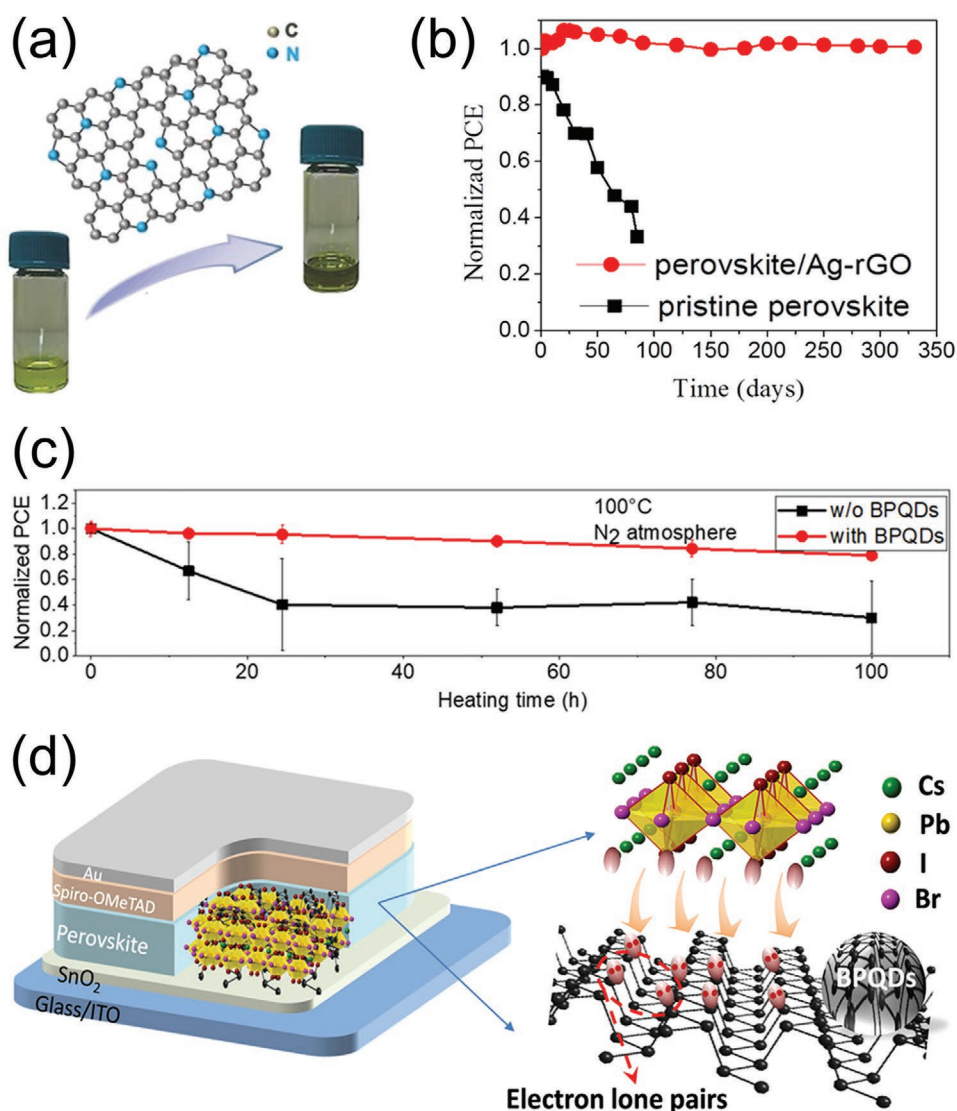
Figure 6. a) Perovskite precursor solution (left) without and (right) with N-rGO nanosheets.[66] Reproduced with permission.[66] Copyright 2016, Wiley-VCH. b) Normalized PCE of Ag-rGO incorporated CH₃NH₃PbI₃₋ₓClₓ perovskite based solar cells over 330 days under ambient condition (25–30 °C, 45–55% humidity).[67] Reproduced with permission.[67] Copyright 2019, American Chemical Society. c) Normalized PCE of the unencapsulated PSCs with and without BPQDs in the PL heated at 100 °C for 100 h in N₂-filled glovebox.[39f] Reproduced with permission.[39f] Copyright 2019, Wiley-VCH. d) Schematic illustration of the device structure and favorable interaction between BPQDs and CsPbI₂Br perovskite.[68] Reproduced with permission.[68] Copyright 2020, American Association for the Advancement of Science.

aged for 330 days at a RH of 45–55% and a temperature of 25–30 °C (Figure 6b). This is an impressive stability result for CH₃NH₃PbI₃₋ₓClₓ perovskite-based solar cells and encourages researchers to advance the development of 2D materials based PSCs. The authors of this work elucidated that the use of Ag-rGO helps to suppress the perovskite degradation and decomposition, while improving interfacial charge transfer. Recently, inverted PSCs were fabricated using rGO-cysteine/nanogold (rGO-CysAu) hybrid incorporated PL.[71] Despite these excellent efforts, these studies have mainly focused on improving the perovskite film of lead based PSCs while lead-free perovskites are appealing because of their less or nontoxicity.[72] This could partially be due to the poor stability and low efficiency of lead-free PSCs. Very recently, Hahn's group achieved

over 13% efficiency for tin-based PSCs by using N-doped GO nanosheets in PL, CTL, and as interfacial layer.[73] The use of N-doped GO the slowed crystallization of Sn-based perovskite and suppressed the Sn²⁺/Sn⁴⁺ oxidation, and resulted in pinhole-free dense perovskite films with large grains. In addition to these improved features, the reduced charge recombination and suitable energy levels were the key factors to the achievement of 13.26% efficiency for lead-free PSCs. More importantly, the unencapsulated lead-free PSCs with N-doped GO incorporated PL exhibited excellent long-term stability, sustaining 91% of the initial PCE over 60 days in ambient air condition (25 °C, 45–50% humidity). This work provides a great inspiration for researchers to develop high efficiency and stable lead-free perovskite-based solar cells using 2D materials. Moreover, **Table 4**

Table 4. PV parameters of PSCs fabricated with monoelemental 2D materials integrated PL and their corresponding device stability and bending tests. Note: the aging and bending test results are presented only for the devices with 2D materials.

Device structure	J_{sc}; [mA cm^{-2}]	V_{oc}; [V]	FF	PCE; [%]	Retained %/aging time/condition	Retained %/bending cycle/radius	Refs.
FTO/cp-TiO$_2$/mp-TiO$_2$/perovskite-N-rGO/Spiro-OMeTAD/Au;	21.80	1.15	0.74	18.7	–	–	[66]
FTO/cp-TiO$_2$/mp-TiO$_2$/perovskite/Spiro-OMeTAD/Au;	20.77	1.12	0.73	17.3			
FTO/cp-TiO$_2$/mp-TiO$_2$/Al$_2$O$_3$/perovskite:Ag-rGO/Spiro-OMeTAD/Au;	23.50	0.93	0.74	16.1	94%/90 h/90 °C; 100%/330 days/at 45–55% RH	–	[67]
ITO/PTAA/CH$_3$NH$_3$PbI$_3$-BPQDs/PCBM/BCP/Ag;	21.90	1.10	0.83	20.0	80%/100 h/100 °C in N$_2$ atmosphere	–	[39f]
ITO/PTAA/CH$_3$NH$_3$PbI$_3$/PCBM/BCP/Ag;	21.20	1.08	0.78	17.7			
ITO/PTAA/CH$_3$NH$_3$PbI$_3$-BPQDs/PCBM/BCP/Ag;	15.86	1.25	0.78	15.5	80%/500 h/at 35–45% RH	–	[68]
ITO/PTAA/CH$_3$NH$_3$PbI$_3$/PCBM/BCP/Ag;	13.23	1.07	0.64	9.26			
ITO/cp-TiO$_2$/perovskite/rGO-4-fluorophenyl/Spiro-OMeTAD/Au	21.50	1.11	0.79	18.8	50%/150 h/1-sun illumination in N$_2$ atmosphere	–	[69]
ITO/cp-TiO$_2$/perovskite/Spiro-OMeTAD/Au	20.10	1.03	0.75	15.6			
FTO/cp-TiO$_2$/mp-TiO$_2$/perovskite/MoS$_2$ QDs:f-RGO/Spiro-OMeTAD/Au	22.49	1.11	0.80	20.1	91%/1032 h/1-sun illumination	–	[70]
FTO/cp-TiO$_2$/mp-TiO$_2$/perovskite/Spiro-OMeTAD/Au	21.49	1.06	0.78	17.5			

summarizes the PV parameters of PSCs employing elemental 2D materials in the PL. The corresponding device stabilities, where applicable, are also provided in Table 4.

Although considerable advancements have been made in integrating graphene derivatives-based additives in PL for PSCs, research into the use of other monoelemental 2D materials in the PL is still at a very early stage. Recent work by Yang et al.[39f] studied the effect of BPQDs additive on the crystal growth and morphology of CH$_3$NH$_3$PbI$_3$ perovskite for solar cells. Because of their superior electronic properties and well compatibility with perovskite, BPQDs increased the perovskite grain size and reduced the nonradiative defect density of the cell while making perovskite films more crystalline. As a result, a PCE of 20% was achieved using the device with BPQDs in the PL, whereas the reference cell without BPQDs showed a maximum efficiency of 17.7%. Interestingly, the perovskite film with BPQDs showed negligible changes after annealing at a temperature of 100 °C in glovebox while the film without BPQDs suffered from severe damages (Figure 6c), revealing that the presence of BPQDs helps to reduce the bulk resistance of the perovskite film. This work successfully revealed that BPQDs are effective additives in CH$_3$NH$_3$PbI$_3$ PL for inverted (p-i-n) PSCs. Recently, Gong et al.[68] further demonstrated the same concept using BPQDs in n-i-p architectured inorganic halide perovskite (CsPbI$_2$Br) based PSCs (Figure 6d). Uniform dispersion of BPQDs in a mixed solvent of N,N'-dimethylformamide (DMF) and dimethyl sulfoxide (DMSO) was prepared using a liquid exfoliation method and were mixed CsPbI$_2$Br perovskite in the same solvent. When BPQDs are incorporated in the PL, the unbonded lone pairs of BPQDs provide excess electrons and favorable interaction with cationic ions in CsPbI$_2$Br (Figure 6d). As a result, effective heterogeneous nucleation sites are formed by the attachment of CsPbI$_2$Br and BPQDs. The fabricated cell achieved an efficiency of 15.47% with an addition of 0.7 wt% BPQDs, while retaining 80% of its initial PCE after aging at a temperature of 28 °C and RH of 35–45% for 500 h. On the other hand, the device without BPQDs showed significantly lower efficiency than the BPQDs@CsPbI$_2$Br based PSCs, while

keeping the only 50% of its initial value under the same aging conditions. This is a pioneering work in developing inorganic halide perovskite-based PV devices with high efficiency and stability using monoelemental 2D materials. Future work should aim to incorporated BP derivatives with lead-free perovskite based solar cells.

Another promising strategy to prepare perovskite film with high crystallinity and improved morphology is to use an effective post-treatment with other materials as interface engineering and surface passivation of the perovskite. In this regard, Wang's group were the first to report the surface passivation of PL using 2D materials (chemically modified GO) as an interlayer to reduce the charge recombination at the interface while enhancing hole extraction.[69] A functional group (4-fluorophenyl) was used to modify the surface of GO. PSCs fabricated with functionalized GO displayed a high PCE of 18.75% with enhanced high V_{oc} value of 1.11 V as compared to its counterpart without GO (15.58% with a V_{oc} of 1.03 V). Later, a PCE of over 20% was achieved by employing a hybrid material consisting of rGO nanosheets and MoS$_2$ quantum dots as an active buffer layer between PL and HTL.[70] Although these studies show great promise in integrating 2D materials with PL for PSCs, efforts on employing monoelemental 2D materials such as antimonene, phosphorene, bismuthene, and others are lacking. Very recently, electrochemical delamination method was used to prepare fluorinated BP (F-BP) nanosheets, which reduced the interfacial traps of the PL due to the a strong hydrogen bond between F$^-$ and MA$^+$/FA$^+$ as well as an ionic bond between F$^-$ and Pb^{2+}.[74] An improved PCE of 22.06% was achieved using the devices with F-BP integrated PL, whereas the control devices without BP/F-BP and with BP-only showed similar efficiencies of around 20%. Impressively, the devices with F-BP showed greatly improved humidity and shelf-life stabilities. The authors attributed these improved stabilities to the excellent ambient stability of F-BP due to the antioxidation and antihydration behavior of fluorine adatoms. However, the as-prepared F-BP showed considerable level of oxidation which may be limiting the potential to maximize the PCE of BP based

Table 5. PV parameters of PSCs with 2D materials-based HTLs and their corresponding device stability and bending tests. Note: the aging and bending test results are presented only for the devices with 2D materials.

Device structure	J_{sc}; [mA cm^{-2}]	V_{oc}; [V]	FF	PCE; [%]	Retained %/ aging time/condition	Retained %/bending cycle/radius	Refs.
ITO/GO/CH$_3$NH$_3$PbI$_{3-x}$Cl$_x$/PCBM/ZnO/Al	17.46	1.00	0.71	12.4	–	–	[81]
ITO/PEDOT:PSS/CH$_3$NH$_3$PbI$_{3-x}$Cl$_x$/PCBM/ZnO/Al	15.09	0.93	0.66	9.26			
ITO/PEDOT:PSS:GO/perovskite/PCBM/ZnO NPs/Ag	21.55	1.02	0.82	18.1	80%/25 days/ambient air	–	[39i]
ITO/PEDOT:PSS/perovskite/PCBM/ZnO NPs/Ag	19.63	0.97	0.79	14.9			
ITO/rGO/CH$_3$NH$_3$PbI$_3$/PCBM/Ag	22.10	0.96	0.77	16.4	60%/1000 h/at 30% RH	70%/150 cycles/5 mm	[39k]
ITO/GO/CH$_3$NH$_3$PbI$_3$/PCBM/Ag	19.50	0.94	0.75	13.8			
ITO/SnO$_2$/perovskite/AF-rGO/Ag	23.30	1.04	0.70	17.0	90%/250 h/at 30% RH	–	[89]
ITO/SnO$_2$/perovskite/Spiro-OMeTAD/Ag	22.80	1.07	0.75	18.2			
ITO/SnO$_2$/perovskite/rGO+Spiro-OMeTAD/Au	23.05	1.11	0.71	18.1	75%/500 h/ambient air	–	[90]
ITO/SnO$_2$/perovskite/Spiro-OMeTAD/Au	22.56	1.10	0.70	17.3			
FTO/cp-TiO$_2$/perovskite/Spiro-OMeTAD/CVD-graphene/Au	21.10	1.09	0.68	15.7	96%/12 h/80 °C;	–	[39o]
FTO/cp-TiO$_2$/perovskite/Spiro- OMeTAD/Au	21.60	1.07	0.72	16.6	94%/96 h/at 45% RH		
ITO/PEDOT:PSS/BPQDs/perovskite/PCBM/ZrAcac/Ag	20.56	1.01	0.80	16.7	–	–	[15b]
ITO/PEDOT:PSS/perovskite/PCBM/ZrAcac/Ag	19.74	0.92	0.78	14.1			
FTO/cp-TiO$_2$/perovskite/BP/Au	17.09	0.84	0.55	7.88	–	–	[39j]
FTO/cp-TiO$_2$/perovskite/Au	14.00	0.59	0.48	4.00			
FTO/cp-TiO$_2$/BP-3/perovskite/BP-1/Spiro-OMeTAD/Ag	23.86	1.12	0.74	19.8	80%/40 days/at 30% RH	–	[93]
FTO/cp-TiO$_2$/perovskite/Spiro-OMeTAD/Ag	22.35	1.08	0.70	16.9			
ITO/PTAA/Phosphorene nanoribbons/MAPbI$_3$/PCBM/BCP/Cu	23.33	1.09	0.83	21.1	–	–	[13c]
ITO/PTAA/MAPbI$_3$/PCBM/BCP/Cu	22.30	1.09	0.81	19.6			
ITO/PTAA/Antimonene/CH$_3$NH$_3$PbI$_3$/PC$_{61}$BM/Bphen/Al	23.52	1.11	0.77	20.1	–	–	[13e]
ITO/PTAA/CH$_3$NH$_3$PbI$_3$/PC$_{61}$BM/Bphen/Al	21.69	1.07	0.76	17.6			

PSCs. Therefore, developing a strategy to better control the oxidation of functionalized BP would be an important area of research to obtain high efficiency and stable PSCs.

3.4. HTL

HTLs have great responsibilities for not only the efficiency of solar cells, but also show significant influence on the device stability. An ideal HTL should fulfill the following requirements: i) high hole mobility and conductivity, ii) suitable energy alignment, iii) low hole trap-density, iv) complete surface coverage, and v) good photochemical stability.[11a,75] 2,2′,7,7′-tetrakis(N,N-di-pmethoxyphenyl-amine)9,9′-spirobifluorene (spiro-OMeTAD) is one of the commonly used HTMs owing to its ability to tick the boxes for above requirements.[76] However, spiro-OMeTAD generally requires other toxic or corrosive chemical dopants such as 4-tert-butylpyridine (4-tbp) and Li salt to improve its hole conductivity for use in solar cells. On the other hand, poly[bis(4-phenyl)(2,4,6-trimethylphenyl)amine (PTAA) is one of the most efficient HTMs due to its high transparency to visible light, excellent conductivity and stability,[77] but the use of PTAA significantly increases the overall device cost. Poly(3,4-ethylenedioxythiophene) polystyrene sulfonate (PEDOT:PSS) is another promising HTM candidate and is often employed in p-i-n PSCs.[78] However, owing to its high energy barrier with PL, the devices constructed based on PEDOT:PSS based HTL suffer from relatively low J_{sc} and V_{oc} values, leading to poor PV performances. Additionally, poly(3-hexylthiophene2,5-diyl) (P3HT) and inorganic NiO$_x$ are feasible HTMs, but improvements

should still be made to maximize the PCE of the corresponding PSCs.[79] Because of their high hole mobilities, conductivities, and excellent mechanical strengths, 2D materials are regarded as suitable candidates to address these issues facing to the typical HTMs for PSCs.[80] In addition, the large surface area of 2D materials was found to show positive effect on the crystallinity of perovskite film, and thus resulting in well-ordered perovskite with large crystalline domains. **Table 5** shows the PV parameters and stability tests of PSCs assembled using 2D materials.

Among various types of 2D materials, graphene and its derivatives have shown specific promise as HTMs in PV devices including PSCs owing to their high conductivity and excellent tunability of their electronic properties. In particular, due to its high oxygen contents, GO shows high work function values which make GO attractive for use in inverted (p-i-n) PSCs. To the best of our knowledge, Sun's group were the first to employ GO as a HTM in inverted planar heterojunction PSCs with CH$_3$NH$_3$PbI$_{3-x}$Cl$_x$ perovskite as a light absorber.[81] In this work, they showed that GO not only acts as a HTM, but the perovskite films grown on GO possess highly textured crystal domains (comparable to PEDOT:PSS) and preferential in-plane orientation of the (110) plane, as confirmed using grazing incidence X-ray diffraction (GIXRD) measurements (see **Figure 7**a,b). By using GO as a HTM, the authors achieved a PCE of up to 12.4% with V_{oc} and FF values of 1 and 0.71 V, respectively. For comparison, the authors also fabricated reference PSCs without HTM and with PEDOT:PSS, which exhibited efficiencies of only 2.64% and 9.26%, respectively. Although the concept of using GO as a HTM in solar cells was well documented in organic PV devices,[82] this work

ADVANCED
SCIENCE NEWS

www.advancedsciencenews.com

ADVANCED
ENERGY
MATERIALS

www.advenergymat.de
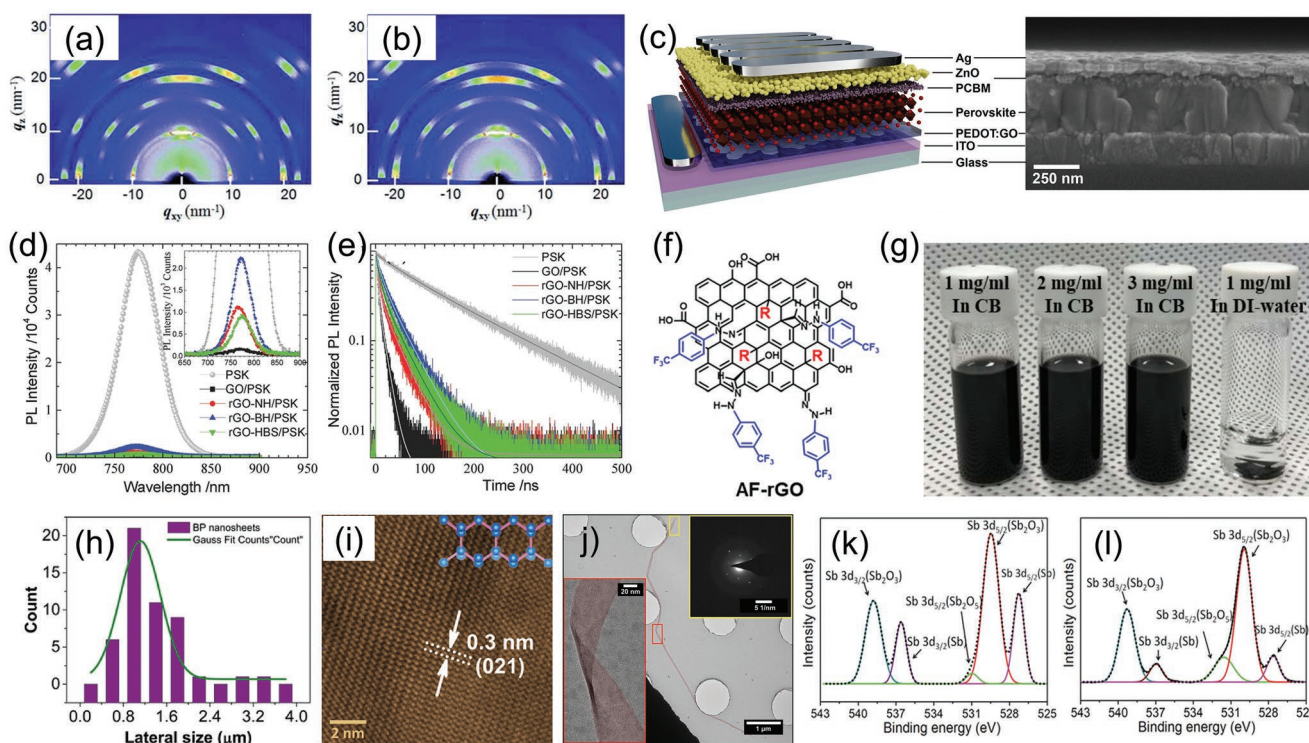
Figure 7. GIXRD profiles of perovskite films grown on a) ITO/GO (≈2 nm) and b) ITO/PEDOT:PSS substrates. Reproduced with permission.[81] Copyright 2019, Royal Society of Chemistry. c) The layered structure and cross-sectional SEM image of the device fabricated using GO incorporated PEDOT:PSS. Reproduced with permission.[39i] Copyright 2019, Royal Society of Chemistry. d) Photoluminescence spectra and e) transient photolumi-nescence decay profiles of perovskite on ITO without and with different HTMs including GO and rGO prepared using three different reducing agents. Reproduced with permission.[39k] Copyright 2018, Wiley-VCH. f) A schematic illustration of alkylated rGO (AF-rGO) structure developed for use as HTM for PSCs. g) Dispersion of AF-rGO in chlorobenzene with different concentrations. Reproduced with permission.[89] Copyright 2021, Wiley-VCH. h) Flake size distribution of BP nanosheets and i) the corresponding HRTEM image. Reproduced with permission.[39j] Copyright 2017, Elsevier B.V. j) TEM image of phosphorene nanoribbon. Inset shows the corresponding selected area electron diffraction pattern (SAED) pattern. Reproduced with permission.[13c] Copyright 2021, American Chemical Society. High resolution X-ray photoelectron (XPS) spectra of k) bulk Sb and l) exfoliated antimonene flakes. Reproduced with permission.[15c] Copyright 2018, Wiley-VCH.

has pioneered recent explorations to develop GO-based PSCs including functionalized GO structures.[39l,83] It is well understood that the wettability issue of PEDOT:PSS films is a serious drawback for depositing uniform layer of perovskite. In this regard, GO shows a great promise as it offers several advantages, but the insulating nature of GO remains to be a major bottleneck when used as a HTM. A simple way to overcome this issue is to combine GO with PEDOT:PSS.[39i,84] For example, Yu et al.[39i] constructed inverted PSCs using a HTL based on GO incorporated PEDOT:PSS (see Figure 7c for device structure). The composite films showed remarkable enhancements in their performances such as good electrical conductivity, suitable energy alignment, reduced series resistance, and excellent crystallinity of the perovskite crystals. These improvements have led to a noticeable increase in the efficiency from 14.95% to 18.09% after incorporating GO in the PEDOT:PSS. Moreover, this device maintained 80% of its initial PCE after being stored in ambient conditions for 25 days, whereas the reference cell without the use of GO in the HTL lost almost 90% of its initial value, demonstrating much slower degradation rate in the presence of GO. Furthermore, due to its high work function (5.2 eV), inserting GO between the PEDOT:PSS and PL was found to improve the PV efficiencies

of inverted devices.[39g] Notably, active buffer layers not only reduce the series resistance of the devices, but also improve the crystallinity of perovskite film.

Since GO nanosheets suffer from poor electrical conductivities, reducing oxygen containing functional groups from GO is a powerful method to obtain highly conductive graphene derivatives.[85] Indeed, Yeo and colleagues reported the first rGO HTM based inverted PSCs.[86] A maximum PCE of 10.8% was achieved using the device with rGO based HTL, while the PSCs with PEDOT:PSS and GO displayed PCEs of 9.14% and 4.04%, respectively. This improvement in the device efficiency was due to the facilitated charge collection caused mainly by the reduced charge recombination, high conductivity, and well-matching energy level of rGO. Furthermore, Jokar et al.[39k] conducted detailed systematic studies on the use of GO and rGO nanosheets as HTMs for inverted PSCs using photoluminescence, transient photoelectric decay, and transient photovoltage decay measurements. They measured that GO was able to extract the holes faster than rGO, where the hole extraction time for GO and rGO was 10.9 and 40.1 ns, respectively (Figure 7d,e). Despite the slower hole extraction time, the device with rGO based HTM showed higher PCE (16.4%) than the GO based PSCs (13.8%). The authors revealed that the abundant number

of localized holes on oxygen atoms were produced rapidly, however the transfer of these localized holes into the ITO electrode was an issue, and thus increased charge recombination has occurred at the interface of perovskite and GO. On the other hand, slower hole injection from perovskite to rGO may have occurred, but the delocalized holes in the benzene rings of rGO reduced the charge recombination within the device. Moreover, both GO and rGO based PSCs showed some promising stabilities over 1000 h at a RH of 30% at 25 °C, both retaining around 60% of their initial PCEs. The authors also demonstrated that flexible PSCs with PCEs of up to 13.8% could be fabricated using rGO based HTMs. The flexible device maintained 70% of its initial PCE over 150 bending cycles.

Although rGO shows some promise as a HTM in these studies, the conductivity, electronic properties, and surface chemistry of rGO nanosheets depend significantly on the reduction routes such as the type of reduction method, reducing agents, and conditions. Therefore, careful control over the reduction of GO is of great importance to obtain rGO nanosheets with desired properties. In particular, the work function of GO can be tuned in a broad range by reducing oxygen containing functional groups,[87] but heavily reduced form of GO can have work function values that are unsuitable for use as a HTM in inverted PSCs. In addition to the changes in these properties, reducing GO increases the hydrophobicity of the structure, making rGO useful as a protection layer for PL in conventional (n-i-p) PSCs. Indeed, Carlo's group employed rGO nanosheets as a HTM to replace spiro-OMeTAD in n-i-p PSCs.[88] The devices with a layered structure of FTO/cp-TiO$_2$/mp-TiO$_2$/perovskite/rGO/Au were fabricated. Interestingly, the initial efficiency of the device fabricated using rGO-only HTM increased from 4.87% to 6.62% after aging almost 2000 h in a shelf. In contrast, the PCE of their reference cell with Spiro-OMeTAD dropped from 11.06% to 6.5% under the same testing condition. Despite the promising stability, the devices fabricated using rGO-based HTM suffered from low PV performances owing to the surface coverage of rGO on PL caused probably by the poor dispersion of rGO in organic solvents. Recently, Park et al.[89] developed alkylated rGO (AF-rGO) nanosheets (Figure 7f), which can be dispersed in chlorobenzene at a high concentration, for PSCs with an n-i-p architecture. Due to the high dispersibility of AF-rGO in nonpolar solvents (Figure 7g), a fully covered AF-rGO film was successfully deposited on top of the PL using a dynamic spin-coating method. As a result, when PSCs were fabricated using AF-rGO as the HTM, the devices exhibited PCEs of up to 17%, which was slightly lower than the efficiency of reference cells with Spiro-OMeTAD (18.2%). Despite its slightly lower efficiency in comparison to Spiro-OMeTAD based PSCs, the device with rGO exhibited an impressive stability in ambient conditions, maintaining almost 90% of its initial PCE after 240 h at a RH of 30%. In comparison, Spiro-OMeTAD based reference cell stopped functioning (0% efficiency) after only 75 h under the same aging condition. The concept of improving device stability using rGO was also demonstrated by Suragtkhuu et al.[90] who first prepared rGO nanosheets from naturally abundant graphite flakes and incorporated them into Spiro-OMeTAD for PSCs. Because of their excellent conductivity and high hydrophobicity, researchers used CVD-grown graphene sheets as a

stabilizer buffer layer between the Spiro-OMeTAD and metal electrode to block the undesirable migration of the metal into the PL.[39o] Although the insertion of graphene lowered the PCE from 16.6% (without graphene) to 15.7%, the device retained 94% of its initial efficiency after aging 96 h in air (45% RH), while the device without graphene lost 43% of its performance. This work demonstrates the possibility of using graphene as an effective protection layer toward the commercialization of PSCs. It is highly anticipated to obtain graphene-based efficient HTMs with excellent hole selectivity by selective doping method to introduce p-type doping effect in graphene structures.

Besides graphene derivatives, other monoelemental 2D materials such as phosphorene and antimonene have recently gained much interest as potential HTMs for PSCs owing to their high charge carrier mobility, ambipolar conduction type, and readily tunable bandgap.[60a,91] The first report on employing BP derivatives as a HTM in PSC was conducted by Chen et al.[15b] who prepared BPQDs using a liquid exfoliation method and inserted them between PEDOT:PSS and PL. In this device structure (ITO/PEDOT:PSS/BPQDs/MAPbI$_3$/PCBM/ZrAcac/Ag), BPQDs acted as a hole extraction layer and improved the PV efficiency of inverted PSCs from 14.1% to 16.69%. The average size of the BP used in this device was only ≈5.2 nm. Soon after, Muduli et al.[39j] reported the preparation of 2D phosphorene flakes with large lateral sizes (Figure 7h) for use as a HTM of n-i-p PSCs by directly replacing Spiro-OMeTAD. It should be noted that the as-prepared phosphorene nanosheets showed a lattice spacing of ≈0.3 nm which can be assigned to the (021) crystal plane. The device with a layered structure of FTO/TiO$_2$/MAPbI$_3$/BP/Au displayed an efficiency of 7.88%, which was significantly higher than that of the cells without HTM (4%), clearly demonstrating the excellent hole selectivity of BP nanosheets. The authors also demonstrate that the efficiency of the reference cells with Spiro-OMeTAD HTM can be enhanced from 13.1% to 16.4% by mixing BP nanosheets with Spiro-OMeTAD. They used photoluminescence quenching and electrochemical impedance spectroscopy (EIS) techniques to confirm the improved charge extraction ability of BP nanosheets. Recently, the concept of adding BP into Spiro-OMeTAD while introducing surface modifications on the perovskite film using halide Cs$_3$TbCl$_6$ quantum dots has seen significant improvement in the V_{oc} value (reaching 1.235 V).[92] Furthermore, by controlling the thickness of BP layers, Zhang et al.[93] were able to tune the bandgap of BP. Therefore, by inserting BP with an appropriate thickness, the authors improved the PCE of PSCs from 16.95% (without BP) to 19.83%. Enhanced light absorption and reduced trap density were the main factors responsible for the improved efficiency of PSCs with BP insertion. In a recent study by Macdonald and colleagues, a novel nanostructure of 2D phosphorene with a range of superlative functional properties was designed.[13c] Phosphorene nanoribbons with a distribution of widths and lengths (typically from 50 nm to 10 µm in length and 5–50 nm in width) were synthesized using sonication based solution processable method (Figure 7j). The highest occupied molecular orbital (HOMO) level and bandgap of the phosphorene nanoribbons were calculated to be ≈5.41 and ≈1.97 eV, respectively, both of which make them highly suitable for use as a HTM in PSCs. Indeed, the authors constructed p-i-n devices by inserting phosphorene nanoribbons between

MAPbI$_3$ perovskite and PTAA layer. A PCE of >21% with a FF value of 0.83 was achieved for the devices with the presence of phosphorene nanoribbons, whereas the control PSCs exhibited an efficiency of up to 19.60%. The authors employed the state-of-the-art characterization techniques such as photoluminescence and transient absorption spectroscopy to reveal that the enhanced hole extraction from perovskite using phosphorene nanoribbons was critical in achieving high PV performances. This work demonstrates that the predicted fascinating properties of BP derivatives translate to improved solar cells.

Antimonene—mono/few layers of antimony (Sb) arranged in a buckled honeycomb architecture—is an appealing 2D semiconductor material with p-type dominated band properties.[31a] Due to their excellent hole density, antimonene nanosheets have shown some promise in the HTL of PSCs. Despite the promise, efforts on using antimonene as a HTM have been very scarce. Indeed, a research team led by Song was the only group who have been working develop PSCs using antimonene nanosheets as the HTM.[15c] In their first work, the authors prepared antimonene flakes using a combination of griding and sonication-assisted liquid exfoliation methods for PSCs. It is well established that the antimonene exhibits thickness-dependent bandgaps. Therefore, the authors of this work were able to tune the bandgap of antimonene from 0.8 and 1.44 eV by changing the centrifugation speed of the exfoliated flakes. Antimonene nanosheets with a bandgap of around 1.4 eV were selected to fabricate p-i-n PSCs with a layered structure of ITO/antimonene/perovskite/PCBM/Bphen/Al. A noticeable enhancement in the hole extraction was observed when antimonene is used as the HTM in the device, leading to around 30% enhancement in the current density in comparison to the HTM-free devices. Although this work demonstrated for the first time that antimonene nanosheets can be used as a HTM of inverted PSCs, the devices delivered limited PV performances. The reason could be explained by the fact that antimonene nanosheets cannot fully cover the underneath surface. This surface coverage issue is one of the main challenges for 2D materials besides the issues associated with scalability and oxidations for device applications.

Furthermore, the same group reported that antimonene can be used as ideal hole extraction layers in planar inverted PSCs.[13e] In their devices, antimonene nanosheets were inserted between the PL and PTAA (HTL). As a result, the PSCs with antimonene layers showed PCEs ranging from 17.58% to 20.11%, while a maximum efficiency of 17.60% was recorded for the control device. The improved efficiency of PSCs in the presence of antimonene layers was attributed to the efficient hole extraction and fast hole transfer at the interface of PL/HTL. The authors of this work further demonstrated in a separate study that efficient, stable and hysteresis-free inverted PSCs can be constructed by employing inorganic HTMs (Cu-doped NiO$_x$) and oxidized antimonene.[94] It was found that the antimonene oxide shows highly suitable energy level alignment with both CH$_3$NH$_3$PbI$_3$ perovskite and Cu-doped NiO$_x$. It can be observed from the X-ray photoelectron (XPS) analysis of these work that both bulk and exfoliated antimonene flakes are oxidized on their surfaces (Figure 7k,l), which are consistent with and highlighted in several recent studies.[24b,95] In this regard, the effect of surface oxidations on the electronic and PV properties of antimonene nanosheets should be investigated and well elucidated.

Based on these studies, it can be concluded that antimonene has been proven excellent candidate as a HTM for solar cells. Importantly, recent computational study showed that the electronic properties of antimonene nanosheets can be tuned to be p-type, n-type or even intrinsic depending on various doping effects.[96] For instance, doping antimonene with Si results in a p-type semiconductor. Therefore, future experimental studies on synthesizing antimonene nanosheets with outstanding p-type properties should focus on introducing different doping effects in the materials. Through this approach, highly efficient PSCs can be developed using doped antimonene nanosheets as the HTM.

3.5. Conductive Back Electrode

In general, a thin layer of conductive metals such as gold (Au), silver (Ag), copper (Cu), and aluminum (Al) is deposited as the back contact to complete the fabrication of PSCs.[97] In addition to the high costs of metal electrodes, the deposition technique using thermal evaporation involves inherently complicated processes. These challenges opened new avenues of research in searching low-cost alternatives to the precious metal electrodes for PSCs. An ideal back electrode for efficient PSCs should meet the following requirements: i) low-cost, ii) high electrical conductivity, iii) suitable energy band alignment, and iv) excellent mechanical stability.[97b] Monoelemental 2D materials with the exception of graphene derivatives cannot fulfill the requirement of high conductivity in PSCs, although they possess highly tunable properties that can satisfy most of the requirements. The first successful effort on fabricating efficient PSCs without metal electrode was reported by Mei et al.[98] who discovered the feasibility of porous carbon as the rear electrode for stable solar cells. The work advanced the field of PSC research by inspiring researchers in the area of carbon materials and PV. However, the poor interface between perovskite and carbon layers has been the key challenge limiting the PCEs of carbon based PSCs. To our knowledge, Yang's group employed rGO as hole extraction electrode in n-i-p PSCs for the first time.[99] Based on ultraviolet photoelectron spectroscopy (UPS) measurements, they determined the work functions of single-layer and multi-layer graphene derivatives to be 4.8 and 5.0 eV, respectively, to find out the suitable interfacial contact regime for hole extraction and charge separation. Moreover, their time resolved photoluminescence (TRPL) measurement showed that multilayer graphene exhibits higher hole extraction rate (5.1 ns^{-1}) than that of the single-layer one (<3.7 ns^{-1}) (**Figure 8**a). Besides its better conductivity as compared to the single-layer structure, multilayer graphene has fewer defective sites within the electrode and thus leading to higher hole extraction rate. As a result, an efficiency of up to 11.5% was achieved using metal-free PSCs with the following device structure: FTO/cp-TiO$_2$/mp-TiO$_2$/perovskite/graphene. Considering the high hydrophobicity of graphene, it is reasonable to expect from this type of devices to show excellent stability in ambient conditions although no stability test was carried out in this work. More importantly, it can be observed from the layered structure of this PSC that the
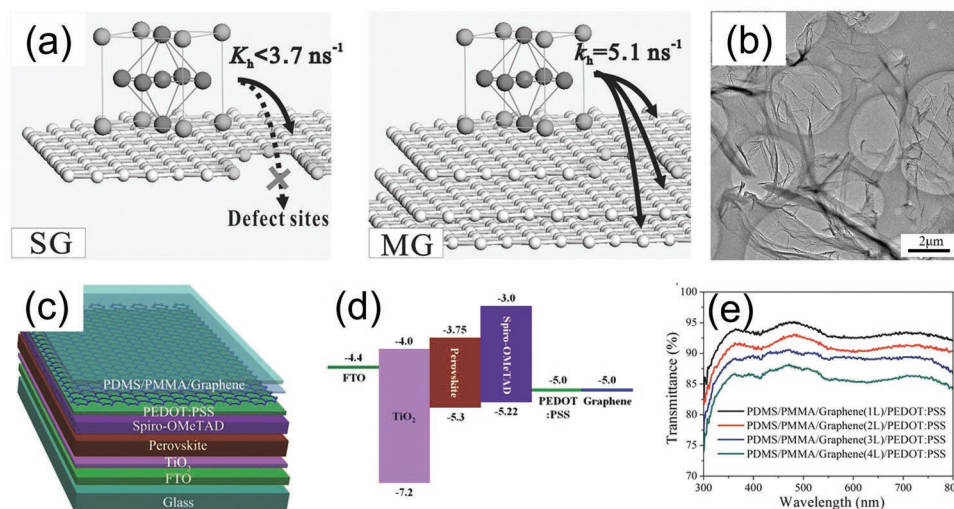
Figure 8. a) Schematic showing the stronger hole extraction ability of multilayer graphene (MG) than single-layer graphene (SG). Reproduced with permission.[99] Copyright 2015, Wiley-VCH. b) TEM image of single-atom Ni and N-doped graphene. Reproduced with permission.[100] Copyright 2021, Elsevier B.V. c) Schematic diagram of a semitransparent PSC constructed using PEDOT:PSS doped PDMS/PMMA/graphene film, and d) the corresponding energy level alignment. e) Transmittances of the graphene films with different layers. Reproduced with permission.[101] Copyright 2015, Wiley-VCH.

graphene electrode is acting as both hole selective and transporting layers, leading to successful fabrication of HTM-free PSCs with reasonable efficiencies. Promisingly, the fabrication of PSCs without HTM and metal electrode would significantly reduce the overall manufacturing cost of the systems. However, due to the limited hole selectivity of carbon materials including graphene, these rear electrodes based PSCs without HTM suffer from poor device performances. Therefore, enhancing hole selectivity and transporting properties of graphene derivatives for PSCs should be explored with a great sense of urgency. **Table 6** summarizes the PV performances and operational stabilities of PSCs employing monoelemental 2D materials-based back electrodes.

Chemical doping is a proven efficient approach to adjust the optoelectronic properties of graphene and other carbonaceous materials.[104] Doping has been shown not only to tune the

energy band alignment of the materials, but it can also improve the electrical conductivity of graphene.[104–105] Indeed, few studies demonstrated improvements in the PV performance of HTM-free and metal-free PSCs fabricated using heteroatom and single-atom doped graphene frameworks.[100,106] For example, Guo et al.[100] recently introduced single-atom Ni onto N-doped graphene (Figure 8b) and employed it as the rear electrode in PSCs. The efficiency of graphene rear electrode based devices increased from 10.99% to 12.39% after the introduction of doping species. The authors used UPS technique to reveal what caused this improvement in the PV performances and found that the Ni- and N-doping can effectively shift the work function of the graphene. Despite the improvement, the PCE of HTM-free and metal-free PSCs using 2D graphene still far from the expectation and efforts should still be made actively in this research area. Besides chemical doping, we anticipate that

Table 6. PV parameters of PSCs fabricated with monoelemental 2D materials-based back electrodes and their corresponding device stability and bending tests. Note: the aging and bending test results are presented only for the devices with 2D materials.

Device structure	J_{sc}; [mA cm^{-2}]	V_{oc}; [V]	FF	PCE; [%]	Retained %/aging time/condition	Retained %/bending cycle/radius	Refs.
FTO/cp-TiO$_2$/mp-TiO$_2$/perovskite/graphene	16.70	0.94	0.73	11.5	–	–	[99]
FTO/SnO$_2$/perovskite/Ni-, N-graphene	20.33	0.95	0.58	12.4	–	–	[100]
FTO/SnO$_2$/perovskite/graphene	18.93	0.94	0.53	10.9			
FTO/cp-TiO$_2$/perovskite/Spiro-OMeTAD/PEDOT:PSS/ PDMS/PMMA/graphene	19.17	0.96	0.67	12.4	–	–	[101]
FTO/cp-TiO$_2$/perovskite/Spiro-OMeTAD/Au	19.80	0.99	0.74	14.4			
FTO/SnO$_2$/perovskite/Spiro-OMeTAD/graphene/ graphene/FTO	22.78	1.05	0.78	18.7	90%/1000 h/85 °C at 40–80% RH	–	[102]
FTO/SnO$_2$/perovskite/Spiro-OMeTAD/Au	22.82	1.12	0.76	19.4			
FTO/cp-TiO$_2$/mp-TiO$_2$/perovskite/Spiro-OMeTAD/ Ti$_1$-rGO/FTO	26.00	1.06	0.79	21.6	95%/1300 h/60 °C under 1-sun illumination in N$_2$ atmosphere	–	[103]
FTO/cp-TiO$_2$/mp-TiO$_2$/perovskite/Spiro-OMeTAD/Au	26.00	1.14	0.79	23.5			

**ADVANCED
SCIENCE NEWS**

www.advancedsciencenews.com

**ADVANCED
ENERGY
MATERIALS**

www.advenergymat.de

heterostructures made of graphene and other monoelemental 2D materials (e.g., phosphorene, antimonene) will be promising candidates for HTM-free and metal-free PSCs as they exhibit excellent p-type properties. For example, constructing a layered structure of phosphorene/graphene or antimonene/graphene would be of great value, but the interfaces between heterostructures and perovskite should be taken into careful consideration.

Since graphene electrodes based PSCs without HTM display limited PV efficiencies, it is reasonable to expect high efficiency devices by using graphene electrodes on top of conventional HTMs, such as Spiro-OMeTAD, P3HT, and PTAA. Graphene films not only show remarkable electrical conductivities, but they also possess excellent optical transparencies. This strategy to construct PSCs using conductive graphene films enables the realization of highly efficient semitransparent devices while being flexible and stable. In 2015, Yan's group developed semitransparent PSCs by laminating graphene transparent electrodes on top of HTL (see device structure from Figure 8c).[101] The authors prepared 1–4 graphene layers on a copper foil using CVD method, followed by coating a thin layer of poly(methyl methacrylate) (PMMA) and attaching a thin poly(dimethylsiloxane) (PDMS) film. Then the PDMS/PMMA/graphene film is ready for deposition to complete the device fabrication. Notably, the electrode conductivity was dramatically increased by depositing a thin layer of PEDOT:PSS onto the PDMS/PMMA/graphene film. Specifically, the sheet resistance of single-layer graphene film decreased from around 1050 to 260 Ω sq^{-1} after doping with PEDOT:PSS. Moreover, it was found that doping graphene with PEDOT:PSS makes it highly suitable for use as electrode material in n-i-p PSCs because of the shift in the Fermi level (Figure 8d).[107] For the best-performing device, two-layer graphene film with a sheet resistance of $\approx$140 Ω sq^{-1} and an optical transmittance of >90% in the visible region was applied (Figure 8e). The device employing PEDOT:PSS doped PDMS/PMMA/graphene electrode delivered a PCE of up to 12.37% with a J_{sc} of 19.17 mA cm^{-2}, V_{oc} of 0.96 V and FF of 0.67, when illuminated from the FTO side. Interestingly, these PV performances were comparable to those obtained using the reference PSCs with Au electrode (14.35%). Remarkably, the authors showed that these graphene films based PSCs can achieve efficiencies higher than 12% with a FF value of 0.72 when illuminated from the graphene side, demonstrating the excellent transparency of the electrode. It is worth mentioning that semitransparent solar cells are sitting in the spotlight as they show great promise for other applications such as tandem PV and BIPVs.[108] The key advantages for using graphene as the rear electrode in PSCs should include the fact that graphene with its high hydrophobic surface is expected to protect the perovskite from moisture induced degradation. Interestingly, during the preparation of this review, we realized that no stability tests were carried out in the majority of these work on graphene electrode based PSCs. Therefore, we strongly encourage that future studies should pay particular attention to the comprehensive stability tests under various conditions.

Recently, Shi and colleagues discovered a novel architecture design to build flexible PSCs using graphene rear electrodes.[102] This innovative modular device design can be assembled using a wide range of carbon back electrode, whose sheet resistance

was greatly reduced by covering it with another carbon coated FTO substrate that was applied under pressure. Impressively, the authors demonstrated that these two individual electrodes could be assembled and disassembled repeatedly. The fabrication steps of modular PSCs using different carbon materials are illustrated in **Figure 9**a. Among various forms of carbon materials, graphene was found to be the material of choice for efficient and stable PSCs without metal electrode. Briefly, two semicells were made, with A being FTO/SnO$_2$/perovskite/graphene. The semicell B was prepared by coating graphene on FTO glass using a spray coating. After assembling, the full device with the structure such as illustrated in Figure 9b was achieved. Remarkably, this device with graphene electrode was able to deliver a PCE of 18.65% which was the best efficiency reported for carbon based PSCs in late-2019. Impressively, the unencapsulated device was able to retain 90% of its initial PV performance after aging at an elevated temperature of 85 °C over 1000 h, whereas the reference cell constructed using metal (Au) electrode lost more than 40% of its initial PCE after only 600 h. This innovative design holds a great promise for the commercialization of PSCs as it not only enables high efficiency and excellent stability, but also the robustness and flexibility of graphene should still be taken into consideration. Very recently, the same authors made a major progress in improving both efficiency and stability of PSCs with graphene electrodes.[103] Instead of using rGO, they introduced a single-atom Ti onto the rGO sheets using rGO sheets and a common chemical (titanium diisopropoxide bis(acetylacetonate) (Figure 9d). It can be seen from electron energy-loss spectroscopy (EELS) analysis that the position of Ti atom corresponds well to that of the C vacancy, revealing that the Ti adatom is strongly anchored into a C-vacancy defect of Ti$_1$–rGO (Figure 9e). As a result, a PCE of up to 21.6% was obtained for the device with single-atom Ti-doped rGO nanosheets based rear electrodes. Notably, this PV efficiency was close to that (23.5%) of the state-of-the-art PSCs fabricated with Au electrode. More importantly, the authors showed that the device with Ti$_1$-rGO electrode was able store 95% of its initial PCE after continuous irradiations under 1 sun for 1300h at a temperature of 60 °C in N$_2$ atmosphere. Although these are harsh testing conditions for PSCs, the authors proved that single-atom doping in graphene and other solid support materials have the great potentials for designing efficient and stable solar cells. Single-atom doping has gained increasing attention in the field of materials science over the past several years due to its ability tune the properties of nanomaterials. However, the application of single-atom doped materials has been limited mainly to catalytic reactions.[109] Therefore, exploring the role and benefits of single-atom doping on the electronic and PV properties of 2D materials would be of great value.

4. Summary

Perovskite light absorbers based solar cells revealed themselves as promising next-generation PV technologies owing to the exponential increase in their PCEs and low manufacturing cost. Although they suffer from poor operational stabilities under harsh conditions such as high humidity, prolonged

ADVANCED
SCIENCE NEWS
www.advancedsciencenews.com

ADVANCED
ENERGY
MATERIALS
www.advenergymat.de
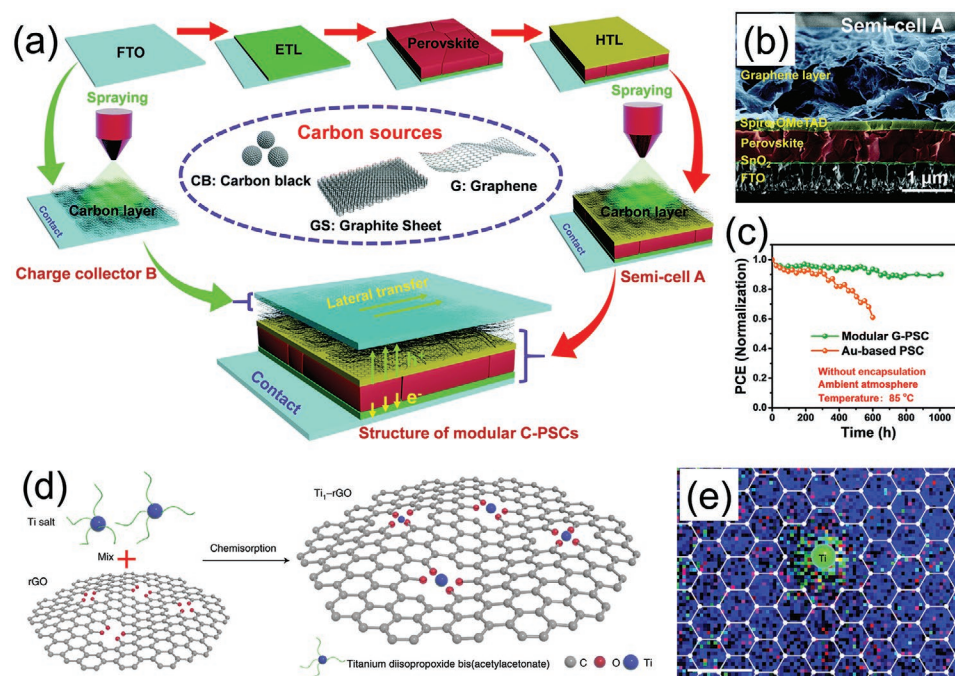
Figure 9. a) Schematic illustration of the fabrication steps for modular PSC using carbon electrodes. b) Cross-sectional SEM image of a modular PSC fabricated using graphene sheets. c) Stability comparison of reference Au-electrode and graphene-based PSCs at 85 °C temperature. Reproduced with permission.[102] Copyright 2019, Royal Society of Chemistry. d) Schematic illustration of the synthesis of single-atom Ti-doped rGO sheet. e) EELS color-coded map of Ti, C, O of Ti_1-rGO, where the green, blue, and red dots represent the distribution of Ti, C, and O elements, respectively. The overlaid schematic represents a possible 2D structural model of Ti_1-rGO. Scale bar: 0.5 nm. Reproduced with permission.[103] Copyright 2021, Springer Nature Limited.

light illumination, and applied heat, excellent progresses have been made in the development of high efficiency, stable PSCs. In this regard, elemental 2D materials such as graphene, phosphorene, antimonene, bismuthene, borophene, and others have been demonstrated to be excellent candidates for different components of PSCs due to their fascinating properties including good optical transparencies, high electrical conductivities, and excellent carrier transport properties. In addition to these attractive features, the most defined and controllable properties of monoelemental 2D materials are their highly tunable electronic properties (e.g., bandgaps, work functions), making them appealing for PV applications. In this review, we have outlined the recent advances and key achievements in the field of PSCs using monoelemental 2D materials. Although excellent progress has been made in this cutting-edge research area over the past several years, there are several concepts remain unclear and further explorations are still required. We believe that the points highlighted below will be of great value and considered carefully in future studies.

5. Perspectives and Roadmaps

i) Graphene-based TCEs hold specific promise for PV devices. However, there has been a major challenge in developing high performance TCEs using solution processed graphene structures. Therefore, new electrode designs using solution processable graphene and other conductive materials, such as metallic nanostructures would be valuable strategy. Chemical

functionalization and doping should be actively explored to develop solution processable graphene-based TCEs with tunable work function and high conductivity. When graphene derivatives are used as TCEs of solar cells, experimental data on the flexibility and robustness of the devices are strongly encouraged to be reported in future studies. Until now, less attention has been paid to the development of tandem solar cells using graphene-based TCEs despite their great potentials.

Since TCEs in solar cells require materials with high electrical conductivities, the use of monoelemental 2D materials such as phosphorene and antimonene as TCE materials for PSCs is not expected. However, these 2D materials with their tunable bandgaps are expected to be valuable interface engineering layers to enhance the charge transport of the solar cells.

ii) Graphene-based structures such as rGO and GO have been promising candidates for enhancing efficiency of various PV devices including PSCs when incorporated in the ETLs. High conductivities or modified work functions were found to be the main reasons behind the efficiency enhancements. Interestingly, few recent studies also revealed that graphene derivatives can also help to improve the device stabilities, but the exact mechanism for improved stabilities is still very unclear and requires further investigations. In addition to its high electrical conductivity, graphene has an outstanding thermal conductivity which makes it promising material for heat dissipation. Therefore, investigating heat dissipation

properties of graphene in PSCs would be valuable research direction.

A range of monoelemental 2D materials including phosphorene, bismuthene, and antimonene show excellent semiconducting properties (e.g., tunable bandgap), making them useful for ETL of solar cells. Although some great efforts have already been made, further improvements in the efficiency of PSCs using these elemental 2D materials in ETLs are highly expected. Since chemical doping can effectively modify the electronic properties of the materials, functionalized 2D materials would be excellent candidates for ETLs of high efficiency PSCs. Notably, progress on using elemental 2D materials as ETMs for flexible devices is very limited.

iii) 2D materials have been widely used for PL mainly to suppress the degradation and decomposition of the perovskite, while also improving the film morphology. These are generally achieved using two different strategies: i) by adding the materials into the perovskite precursor solution before film preparation, and ii) by using 2D materials as interface engineering layer and perovskite surface passivator. Based on recent studies, it can be noted that interface engineering or surface passivation approach is very effective in achieving high device performance. However, applying monoelemental 2D materials as surface passivator is still at an infant stage; and efforts should actively be made in this research area. In addition, future studies should aim to design high performance lead-free perovskite films for PSCs. We anticipate that 2D materials will play important roles in lead-free perovskite based solar cells. However, the oxidation issues of monoelemental 2D materials such as phosphorene, antimonene, and bismuthene should be considered carefully.

iv) Because of their high hole mobilities, p-type dominated electronic properties and tunable bandgaps, the majority of monoelemental 2D materials are considered as excellent candidates for HTM of solar cells. However, graphene and phosphorene-based materials are mainly employed as HTMs in PSCs. Although great efforts have been made over the past several years, further improvements in both efficiency and stability of PSCs are highly expected by carefully tuning the work function of graphene-based materials.

The major challenges in employing 2D materials as HTMs include oxidation, scalability, and surface coverage of the materials. To address the surface coverage issue, developing new controllable designs to prepare 2D materials with full coverage is of great importance. Moreover, the production of 2D materials with large lateral sizes will be valuable. The oxidation effects on the electronic properties of monoelemental 2D materials, particularly phosphorene and antimonene, should be systematically studied.

v) Pure graphene structures have excellent hydrophobicity which often helps to achieve highly stable PSCs. However, graphene sheets without any surface functionalization suffer to disperse in common solvents and thus resulting in difficulties to prepare good electrodes. Moreover, the functional groups of graphene also help to improve the hole

selectivity and transporting properties for solar cells. Therefore, achieving an optimal functionalization in graphene is the key to design HTM-free and metal-free PSCs with high efficiency and excellent stability. The development of PSCs without HTM and metal electrode will reduce the overall device cost. In addition to functionalization strategies, carefully built 2D/2D heterostructures with good interface will be promising materials for PSCs. Particularly, the use of p-type 2D materials such as phosphorene is expected to provide outstanding features. Graphene back electrodes are promising candidates for designing semitransparent and flexible PSCs, but limited efforts have been made until now. Moreover, the main advantage of graphene electrodes in PSCs is that they can be used to construct highly stable devices. However, we noticed that no stability tests have been conducted in recent studies on graphene rear electrode based PSCs.

Acknowledgements

Conflict of Interest

The authors declare no conflict of interest.

Keywords

[1] D. Gielen, F. Boshell, D. Saygin, M. D. Bazilian, N. Wagner, R. Gorini, *Energy Strategy Rev.* **2019**, *24*, 38.

[2] International-Energy-Agency, https://www.iea.org/news/pathway-to-critical-and-formidable-goal-of-net-zero-emissions-by-2050-is-narrow-but-brings-huge-benefits. **2021** (accessed: November 2022).

[3] a) C. Battaglia, A. Cuevas, S. De Wolf, *Energy Environ. Sci.* **2016**, *9*, 1552; b) R. Saive, *Prog. Photovoltaics* **2021**, *29*, 1125.

[4] P. Myagmarsereejid, M. Ingram, M. Batmunkh, Y. L. Zhong, *Small* **2021**, *17*, 2100241.

[5] A. R. Barron, *Mater. Today* **2015**, *18*, 2.

[6] F. Fu, J. Li, T. C.-J. Yang, H. Liang, A. Faes, Q. Jeangros, C. Ballif, Y. Hou, *Adv. Mater.* **2022**, *34*, 2106540.

[7] C. Wu, K. Wang, M. Batmunkh, A. S. R. Bati, D. Yang, Y. Jiang, Y. Hou, J. G. Shapter, S. Priya, *Nano Energy* **2020**, *70*, 104480.

[8] a) J. Y. Kim, J.-W. Lee, H. S. Jung, H. Shin, N.-G. Park, *Chem. Rev.* **2020**, *120*, 7867; b) D. Li, D. Zhang, K.-S. Lim, Y. Hu, Y. Rong, A. Mei, N.-G. Park, H. Han, *Adv. Funct. Mater.* **2021**, *31*, 2008621.

[9] L. Meng, J. You, Y. Yang, *Nat. Commun.* **2018**, *9*, 5265.

[10] a) A. Kojima, K. Teshima, Y. Shirai, T. Miyasaka, *J. Am. Chem. Soc.* **2009**, *131*, 6050; b) National-Renewable-Energy-Laboratory, https://www.nrel.gov/pv/assets/pdfs/best-research-cell-efficiencies-rev220630.pdf (accessed: November 2022).

[11] a) A. S. R. Bati, M. Batmunkh, J. G. Shapter, *Adv. Energy Mater.* **2020**, *10*, 1902253; b) Z. Qin, Y. Chen, K. Zhu, Y. Zhao, *ACS Mater. Lett.* **2021**, *3*, 1402.

[12] S. Pescetelli, A. Agresti, G. Viskadouros, S. Razza, K. Rogdakis, I. Kalogerakis, E. Spiliarotis, E. Leonardi, P. Mariani, L. Sorbello, M. Pierro, C. Cornaro, S. Bellani, L. Najafi, B. Martín-García, A. E. Del Rio Castillo, R. Oropesa-Nuñez, M. Prato, S. Maranghi, M. L. Parisi, A. Sinicropi, R. Basosi, F. Bonaccorso, E. Kymakis, A. Di Carlo, *Nat. Energy* **2022**, *7*, 597.

[13] a) M. Acik, S. B. Darling, *J. Mater. Chem. A* **2016**, *4*, 6185; b) Y. Zhang, L. Wang, L. Zhao, K. Wang, Y. Zheng, Z. Yuan, D. Wang, X. Fu, G. Shen, W. J. A. M. Han, **2021**, *33*, 2007890; c) T. J. Macdonald, A. J. Clancy, W. Xu, Z. Jiang, C.-T. Lin, L. Mohan, T. Du, D. D. Tune, L. Lanzetta, G. Min, T. Webb, A. Ashoka, R. Pandya, V. Tileli, M. A. McLachlan, J. R. Durrant, S. A. Haque, C. A. Howard, *J. Am. Chem. Soc.* **2021**, *143*, 21549; d) A. Zhao, Y. Han, Y. Che, Q. Liu, X. Wang, Q. Li, J. Sun, Z. Lei, X. He, Z.-H. Liu, *J. Mater. Chem. A* **2021**, *9*, 24036; e) F. Zhang, J. He, Y. Xiang, K. Zheng, B. Xue, S. Ye, X. Peng, Y. Hao, J. Lian, P. Zeng, J. Qu, J. Song, *Adv. Mater.* **2018**, *30*, 1803244.

[14] J. T.-W. Wang, J. M. Ball, E. M. Barea, A. Abate, J. A. Alexander-Webber, J. Huang, M. Saliba, I. Mora-Sero, J. Bisquert, H. J. Snaith, R. J. Nicholas, *Nano Lett.* **2014**, *14*, 724.

[15] a) P. Ares, F. Aguilar-Galindo, D. Rodríguez-San-Miguel, D. A. Aldave, S. Díaz-Tendero, M. Alcamí, F. Martín, J. Gómez-Herrero, F. Zamora, *Adv. Mater.* **2016**, *28*, 6332; b) W. Chen, K. Li, Y. Wang, X. Feng, Z. Liao, Q. Su, X. Lin, Z. He, *J. Phys. Chem. Lett.* **2017**, *8*, 591; c) X. Wang, J. He, B. Zhou, Y. Zhang, J. Wu, R. Hu, L. Liu, J. Song, J. Qu, *Angew. Chem., Int. Ed.* **2018**, *57*, 8668; d) R. Xue, X. Zhou, S. Peng, P. Xu, S. Wang, C. Xu, W. Zeng, Y. Xiong, D. Liang, *ACS Sustainable Chem. Eng.* **2020**, *8*, 10714.

[16] a) K. Liu, S. Chen, J. Wu, H. Zhang, M. Qin, X. Lu, Y. Tu, Q. Meng, X. Zhan, *Energy Environ. Sci.* **2018**, *11*, 3463; b) G. Yang, H. Lei, H. Tao, X. Zheng, J. Ma, Q. Liu, W. Ke, Z. Chen, L. Xiong, P. Qin, Z. Chen, M. Qin, X. Lu, Y. Yan, G. Fang, *Small* **2017**, *13*, 1601769.

[17] H.-S. Kim, N.-G. Park, *J. Phys. Chem. Lett.* **2014**, *5*, 2927.

[18] a) M. Y. Woo, K. Choi, J. H. Lee, S. Y. Park, J. H. Noh, *Adv. Energy Mater.* **2021**, *11*, 2003119; b) Y. Li, H. Xie, E. L. Lim, A. Hagfeldt, D. Bi, *Adv. Energy Mater.* **2022**, *12*, 2102730.

[19] J. Huang, K.-X. Wang, J.-J. Chang, Y.-Y. Jiang, Q.-S. Xiao, Y. Li, *J. Mater. Chem. A* **2017**, *5*, 13817.

[20] H. J. Snaith, M. Grätzel, *Appl. Phys. Lett.* **2006**, *89*, 262114.

[21] a) Z. He, Y. Zhou, A. Liu, L. Gao, C. Zhang, G. Wei, T. Ma, *Nanoscale* **2021**, *13*, 17272; b) L. Lin, T. W. Jones, T. C.-J. Yang, N. W. Duffy, J. Li, L. Zhao, B. Chi, X. Wang, G. J. Wilson, *Adv. Funct. Mater.* **2021**, *31*, 2008300; c) Y. Yao, C. Cheng, C. Zhang, H. Hu, K. Wang, S. De Wolf, *Adv. Mater.* **2022**, *34*, 2203794.

[22] a) G. R. Bhimanapati, Z. Lin, V. Meunier, Y. Jung, J. Cha, S. Das, D. Xiao, Y. Son, M. S. Strano, V. R. Cooper, L. Liang, S. G. Louie, E. Ringe, W. Zhou, S. S. Kim, R. R. Naik, B. G. Sumpter, H. Terrones, F. Xia, Y. Wang, J. Zhu, D. Akinwande, N. Alem, J. A. Schuller, R. E. Schaak, M. Terrones, J. A. Robinson, *ACS Nano* **2015**, *9*, 11509; b) S. Z. Butler, S. M. Hollen, L. Cao, Y. Cui, J. A. Gupta, H. R. Gutiérrez, T. F. Heinz, S. S. Hong, J. Huang, A. F. Ismach, E. Johnston-Halperin, M. Kuno, V. V. Plashnitsa, R. D. Robinson, R. S. Ruoff, S. Salahuddin, J. Shan, L. Shi, M. G. Spencer, M. Terrones, W. Windl, J. E. Goldberger, *ACS Nano* **2013**, *7*, 2898.

[23] K. S. Novoselov, A. K. Geim, S. V. Morozov, D. Jiang, Y. Zhang, S. V. Dubonos, I. V. Grigorieva, A. A. Firsov, *Science* **2004**, *306*, 666.

[24] a) P. Myagmarsereejid, M. Bat-Erdene, A. S. R. Bati, B. Sainbileg, M. Hayashi, J. G. Shapter, Y. L. Zhong, M. Batmunkh, *ACS Appl. Nano Mater.* **2022**, *5*, 12107; b) M. Bat-Erdene, P. Myagmarsereejid, A. S. R. Bati, J. Qin, Y. L. Zhong, J. G. Shapter, M. Batmunkh, *Small Struct.* **2022**, *3*, 2200038; c) M. Xu, T. Liang, M. Shi, H. Chen, *Chem. Rev.* **2013**, *113*, 3766; d) M. Bernardi, M. Palummo, J. C. Grossman, *Nano Lett.* **2013**, *13*, 3664; e) R. Singh, A. Giri, M. Pal, K. Thiyagarajan, J. Kwak, J.-J. Lee, U. Jeong, K. Cho, *J. Mater. Chem. A* **2019**, *7*, 7151.

[25] V. Nicolosi, M. Chhowalla, M. G. Kanatzidis, M. S. Strano, J. N. Coleman, *Science* **2013**, *340*, 1226419.

[26] a) Y. Liang, V. Wang, H. Mizuseki, Y. Kawazoe, *J. Phys.: Condens. Matter* **2012**, *24*, 455302; b) J. Kim, S. S. Baik, S. H. Ryu, Y. Sohn, S. Park, B.-G. Park, J. Denlinger, Y. Yi, H. J. Choi, K. S. Kim, *Science* **2015**, *349*, 723.

[27] M. Batmunkh, M. Bat-Erdene, J. G. Shapter, *Adv. Mater.* **2016**, *28*, 8586.

[28] a) I. Jung, D. A. Dikin, R. D. Piner, R. S. Ruoff, *Nano Lett.* **2008**, *8*, 4283; b) Z. Wei, D. Wang, S. Kim, S.-Y. Kim, Y. Hu, M. K. Yakes, A. R. Laracuente, Z. Dai, S. R. Marder, C. Berger, W. P. King, W. A. de Heer, P. E. Sheehan, E. Riedo, *Science* **2010**, *328*, 1373; c) S. Gupta, P. Joshi, J. Narayan, *Carbon* **2020**, *170*, 327.

[29] a) M. A. Velasco-Soto, S. A. Pérez-García, J. Alvarez-Quintana, Y. Cao, L. Nyborg, L. Licea-Jiménez, *Carbon* **2015**, *93*, 967; b) H. Huang, Z. Li, J. She, W. Wang, *J. Appl. Phys.* **2012**, *111*, 054317.

[30] a) F. R. Fan, R. Wang, H. Zhang, W. Wu, *Chem. Soc. Rev.* **2021**, *50*, 10983; b) H. Liu, Y. Du, Y. Deng, P. D. Ye, *Chem. Soc. Rev.* **2015**, *44*, 2732.

[31] a) M. Bat-Erdene, A. S. R. Bati, J. Qin, H. Zhao, Y. L. Zhong, J. G. Shapter, M. Batmunkh, *Adv. Funct. Mater.* **2022**, *32*, 2107280; b) S. Zhang, W. Zhou, Y. Ma, J. Ji, B. Cai, S. A. Yang, Z. Zhu, Z. Chen, H. Zeng, *Nano Lett.* **2017**, *17*, 3434; c) S. Zhang, M. Xie, F. Li, Z. Yan, Y. Li, E. Kan, W. Liu, Z. Chen, H. Zeng, *Angew. Chem., Int. Ed.* **2016**, *55*, 1666.

[32] X. Tang, J. Gu, J. Shang, Z. Chen, L. Kou, *InfoMat* **2021**, *3*, 327.

[33] W. Zhong, Y. Zhao, B. Zhu, J. Sha, E. S. Walker, S. Bank, Y. Chen, D. Akinwande, L. Tao, *Nanotechnology* **2020**, *31*, 475202.

[34] a) Z. Wang, H. Kim, H. N. Alshareef, *Adv. Mater.* **2018**, *30*, 1706656; b) K. Hantanasirisakul, Y. Gogotsi, *Adv. Mater.* **2018**, *30*, 1804779; c) A. Lipatov, H. Lu, M. Alhabeb, B. Anasori, A. Gruverman, Y. Gogotsi, A. Sinitskii, *Sci. Adv.* **2018**, *4*, eaat0491; d) G. Li, K. Kushnir, Y. Dong, S. Chertopalov, A. M. Rao, V. N. Mochalin, R. Podila, L. V. Titova, *2D Mater.* **2018**, *5*, 035043.

[35] a) L. Kou, C. Chen, S. C. Smith, *J. Phys. Chem. Lett.* **2015**, *6*, 2794; b) D. Akinwande, N. Petrone, J. Hone, *Nat. Commun.* **2014**, *5*, 5678; c) Q. H. Wang, K. Kalantar-Zadeh, A. Kis, J. N. Coleman, M. S. Strano, *Nat. Nanotechnol.* **2012**, *7*, 699; d) W. Huang, H. Da, G. Liang, *J. Appl. Phys.* **2013**, *113*, 104304.

[36] a) S. Jo, N. Ubrig, H. Berger, A. B. Kuzmenko, A. F. Morpurgo, *Nano Lett.* **2014**, *14*, 2019; b) K. Liu, Q. Yan, M. Chen, W. Fan, Y. Sun, J. Suh, D. Fu, S. Lee, J. Zhou, S. Tongay, J. Ji, J. B. Neaton, J. Wu, *Nano Lett.* **2014**, *14*, 5097.

[37] C. Wan, X. Gu, F. Dang, T. Itoh, Y. Wang, H. Sasaki, M. Kondo, K. Koga, K. Yabuki, G. J. Snyder, R. Yang, K. Koumoto, *Nat. Mater.* **2015**, *14*, 622.

[38] L. Li, Y. Yu, G. J. Ye, Q. Ge, X. Ou, H. Wu, D. Feng, X. H. Chen, Y. Zhang, *Nat. Nanotechnol.* **2014**, *9*, 372.

[39] a) J. A. Hong, E. D. Jung, J. C. Yu, D. W. Kim, Y. S. Nam, I. Oh, E. Lee, J.-W. Yoo, S. Cho, M. H. Song, *ACS Appl. Mater. Interfaces* **2020**, *12*, 2417; b) A. S. R. Bati, L. Yu, M. Batmunkh, J. G. Shapter, *Adv. Funct. Mater.* **2019**, *29*, 1902273; c) X. Zhao, L. Tao, H. Li,

ADVANCED
SCIENCE NEWS

www.advancedsciencenews.com

ADVANCED
ENERGY
MATERIALS

www.advenergymat.de

W. Huang, P. Sun, J. Liu, S. Liu, Q. Sun, Z. Cui, L. Sun, Y. Shen, Y. Yang, M. Wang, *Nano Lett.* **2018**, *18*, 2442; d) M. Batmunkh, K. Vimalanathan, C. Wu, A. S. R. Bati, L. Yu, S. A. Tawfik, M. J. Ford, T. J. Macdonald, C. L. Raston, S. Priya, C. T. Gibson, J. G. Shapter, *Small Methods* **2019**, *3*, 1800521; e) B. Gu, Y. Du, B. Chen, R. Zhao, H. Lu, Q. Xu, C. Guo, *ACS Appl. Mater. Interfaces* **2022**, *14*, 11264; f) W. Yang, J. Chen, X. Lian, J. Li, F. Yao, G. Wu, C. Qiu, C. Jin, P. Heremans, H. Chen, *Sol. RRL* **2019**, *3*, 1900132; g) Y. Wang, S. Wang, X. Chen, Z. Li, J. Wang, T. Li, X. Deng, *J. Mater. Chem. A* **2018**, *6*, 4860; h) N. Fu, C. Huang, P. Lin, M. Zhu, T. Li, M. Ye, S. Lin, G. Zhang, J. Du, C. Liu, B. Xu, D. Wang, S. Ke, *J. Mater. Chem. A* **2018**, *6*, 8886; i) J. C. Yu, J. A. Hong, E. D. Jung, D. B. Kim, S.-M. Baek, S. Lee, S. Cho, S. S. Park, K. J. Choi, M. H. Song, *Sci. Rep.* **2018**, *8*, 1070; j) S. K. Muduli, E. Varrla, S. A. Kulkarni, G. Han, K. Thirumal, O. Lev, S. Mhaisalkar, N. Mathews, *J. Power Sources* **2017**, *371*, 156; k) E. Jokar, Z. Y. Huang, S. Narra, C.-Y. Wang, V. Kattoor, C.-C. Chung, E. W.-G. Diau, *Adv. Energy Mater.* **2018**, *8*, 1701640; l) Q.-D. Yang‡, J. Li, Y. Cheng, H.-W. Li, Z. Guan, B. Yu, S.-W. Tsang, *J. Mater. Chem. A* **2017**, *5*, 9852; m) J. Yoon, H. Sung, G. Lee, W. Cho, N. Ahn, H. S. Jung, M. Choi, *Energy Environ. Sci.* **2017**, *10*, 337; n) V.-D. Tran, S. V. N. Pammi, B.-J. Park, Y. Han, C. Jeon, S.-G. Yoon, *Nano Energy* **2019**, *65*, 104018; o) X. Hu, H. Jiang, J. Li, J. Ma, D. Yang, Z. Liu, F. Gao, S. Liu, *Nanoscale* **2017**, *9*, 8274; p) J. H. Heo, D. H. Shin, D. H. Song, D. H. Kim, S. J. Lee, S. H. Im, *J. Mater. Chem. A* **2018**, *6*, 8251; q) S. H. Shin, D. H. Shin, S.-H. Choi, *ACS Sustainable Chem. Eng.* **2019**, *7*, 13178; r) G. Jeong, D. Koo, J. Seo, S. Jung, Y. Choi, J. Lee, H. Park, *Nano Lett.* **2020**, *20*, 3718.

[40] Y. Ma, L. Zhi, *Small Methods* **2019**, *3*, 1800199.

[41] L. Yu, C. Shearer, J. Shapter, *Chem. Rev.* **2016**, *116*, 13413.

[42] J. Kim, J. W. Lim, F. M. Mota, J.-E. Lee, R. Boppella, K. Y. Lim, K. Kim, W. K. Choi, D. H. Kim, *Nanoscale* **2016**, *8*, 18938.

[43] a) Y. Chen, X.-L. Gong, J.-G. Gai, *Adv. Sci.* **2016**, *3*, 1500343; b) M. Batmunkh, M. J. Biggs, J. G. Shapter, *Small* **2015**, *11*, 2963.

[44] H. Sung, N. Ahn, M. S. Jang, J.-K. Lee, H. Yoon, N.-G. Park, M. Choi, *Adv. Energy Mater.* **2016**, *6*, 1501873.

[45] M. Batmunkh, C. J. Shearer, M. J. Biggs, J. G. Shapter, *J. Mater. Chem. A* **2016**, *4*, 2605.

[46] J. H. Heo, D. H. Shin, S. Kim, M. H. Jang, M. H. Lee, S. W. Seo, S.-H. Choi, S. H. Im, *Chem. Eng. J.* **2017**, *323*, 153.

[47] a) Z. Liu, S. P. Lau, F. Yan, *Chem. Soc. Rev.* **2015**, *44*, 5638; b) Y. Song, W. Fang, R. Brenes, J. Kong, *Nano Today* **2015**, *10*, 681.

[48] a) H.-J. Kim, S.-H. Lee, J. Lee, E.-S. Lee, J.-H. Choi, J.-H. Jung, J.-Y. Jung, D.-G. Choi, *Small* **2014**, *10*, 3767; b) I. E. Stewart, S. Ye, Z. Chen, P. F. Flowers, B. J. Wiley, *Chem. Mater.* **2015**, *27*, 7788.

[49] a) H. J. Snaith, A. Abate, J. M. Ball, G. E. Eperon, T. Leijtens, N. K. Noel, S. D. Stranks, J. T.-W. Wang, K. Wojciechowski, W. Zhang, *J. Phys. Chem. Lett.* **2014**, *5*, 1511; b) J. P. Correa Baena, L. Steier, W. Tress, M. Saliba, S. Neutzner, T. Matsui, F. Giordano, T. J. Jacobsson, A. R. Srimath Kandada, S. M. Zakeeruddin, A. Petrozza, A. Abate, M. K. Nazeeruddin, M. Grätzel, A. Hagfeldt, *Energy Environ. Sci.* **2015**, *8*, 2928; c) Y. Lin, Y. Shen, J. Dai, Y. Deng, Y. Wu, Y. Bai, X. Zheng, J. Wang, Y. Fang, H. Wei, W. Ma, X. C. Zeng, X. Zhan, J. Huang, *Adv. Mater.* **2017**, *29*, 1604545; d) J. Lian, B. Lu, F. Niu, P. Zeng, X. Zhan, *Small Methods* **2018**, *2*, 1800082.

[50] D. Wang, T. Ye, Y. Zhang, *J. Mater. Chem. A* **2020**, *8*, 20819.

[51] a) Q. Jiang, X. Zhang, J. You, *Small* **2018**, *14*, 1801154; b) Y. Jiang, J. Wang, H. Zai, D. Ni, J. Wang, P. Xue, N. Li, B. Jia, H. Lu, Y. Zhang, F. Wang, Z. Guo, Z. Bi, H. Xie, Q. Wang, W. Ma, Y. Tu, H. Zhou, X. Zhan, *J. Am. Chem. Soc.* **2022**, *144*, 5400; c) M. Zhang, X. Zhan, *Adv. Energy Mater.* **2019**, *9*, 1900860.

[52] a) M. Batmunkh, M. J. Biggs, J. G. Shapter, *Adv. Sci.* **2015**, *2*, 1400025; b) J. D. Roy-Mayhew, I. A. Aksay, *Chem. Rev.* **2014**, *114*, 6323.

[53] G. S. Han, Y. H. Song, Y. U. Jin, J.-W. Lee, N.-G. Park, B. K. Kang, J.-K. Lee, I. S. Cho, D. H. Yoon, H. S. Jung, *ACS Appl. Mater. Interfaces* **2015**, *7*, 23521.

[54] A. Agresti, S. Pescetelli, L. Cinà, D. Konios, G. Kakavelakis, E. Kymakis, A. D. Carlo, *Adv. Funct. Mater.* **2016**, *26*, 2686.

[55] a) A. Agresti, S. Pescetelli, A. L. Palma, B. Martín-García, L. Najafi, S. Bellani, I. Moreels, M. Prato, F. Bonaccorso, A. Di Carlo, *ACS Energy Lett.* **2019**, *4*, 1862; b) F. Biccari, F. Gabelloni, E. Burzi, M. Gurioli, S. Pescetelli, A. Agresti, A. E. Del Rio Castillo, A. Ansaldo, E. Kymakis, F. Bonaccorso, A. Di Carlo, A. Vinattieri, *Adv. Energy Mater.* **2017**, *7*, 1701349; c) A. Agresti, S. Pescetelli, A. L. Palma, A. E. Del Rio, Castillo, D. Konios, G. Kakavelakis, S. Razza, L. Cinà, E. Kymakis, F. Bonaccorso, A. DiCarlo, *ACS Energy Lett.* **2017**, *2*, 279; d) E. Lamanna, F. Matteocci, E. Calabrò, L. Serenelli, E. Salza, L. Martini, F. Menchini, M. Izzi, A. Agresti, S. Pescetelli, S. Bellani, A. E. Del Río, Castillo, F. Bonaccorso, M. Tucci, A. DiCarlo, *Joule* **2020**, *4*, 865.

[56] P. O'Keeffe, D. Catone, A. Paladini, F. Toschi, S. Turchini, L. Avaldi, F. Martelli, A. Agresti, S. Pescetelli, A. E. Del Rio, Castillo, F. , Bonaccorso, A. , DiCarlo , *Nano Lett.* **2019**, *19*, 684.

[57] a) Q. Jiang, L. Zhang, H. Wang, X. Yang, J. Meng, H. Liu, Z. Yin, J. Wu, X. Zhang, J. You, *Nat. Energy* **2016**, *2*, 16177; b) W. Ke, G. Fang, Q. Liu, L. Xiong, P. Qin, H. Tao, J. Wang, H. Lei, B. Li, J. Wan, G. Yang, Y. Yan, *J. Am. Chem. Soc.* **2015**, *137*, 6730.

[58] J. Xie, K. Huang, X. Yu, Z. Yang, K. Xiao, Y. Qiang, X. Zhu, L. Xu, P. Wang, C. Cui, D. Yang, *ACS Nano* **2017**, *11*, 9176.

[59] J. Si, J. Yu, Y. Shen, M. Zeng, L. Fu, *Small Struct.* **2021**, *2*, 2000101.

[60] a) M. Batmunkh, M. Bat-Erdene, J. G. Shapter, *Adv. Energy Mater.* **2018**, *8*, 1701832; b) M. Bat-Erdene, M. Batmunkh, S. A. Tawfik, M. Fronzi, M. J. Ford, C. J. Shearer, L. Yu, M. Dadkhah, J. R. Gascooke, C. T. Gibson, J. G. Shapter, *Adv. Funct. Mater.* **2017**, *27*, 1704488.

[61] T. Chai, X. Li, T. Feng, P. Guo, Y. Song, Y. Chen, H. Zhang, *Nanoscale* **2018**, *10*, 17617.

[62] Y. V. Kaneti, D. P. Benu, X. Xu, B. Yuliarto, Y. Yamauchi, D. Golberg, *Chem. Rev.* **2022**, *122*, 1000.

[63] a) C. Zhang, Y. Li, P. Zhang, M. Qiu, X. Jiang, H. Zhang, *Sol. Energy Mater. Sol. Cells* **2019**, *189*, 11; b) Z. Wang, R. Zhang, M. Zhao, Z. Wang, B. Wei, X. Zhang, S. Feng, H. Cao, P. Liu, Y. Hao, H. Wang, B. Xu, S. J. Pennycook, J. Guo, *J. Mater. Chem. A* **2018**, *6*, 23773.

[64] W. Nie, H. Tsai, R. Asadpour, J.-C. Blancon, A. J. Neukirch, G. Gupta, J. J. Crochet, M. Chhowalla, S. Tretiak, M. A. Alam, H.-L. Wang, A. D. Mohite, *Science* **2015**, *347*, 522.

[65] F. Zhang, K. Zhu, *Adv. Energy Mater.* **2020**, *10*, 1902579.

[66] M. Hadadian, J.-P. Correa-Baena, E. K. Goharshadi, A. Ummadisingu, J.-Y. Seo, J. Luo, S. Gholipour, S. M. Zakeeruddin, M. Saliba, A. Abate, M. Grätzel, A. Hagfeldt, *Adv. Mater.* **2016**, *28*, 8681.

[67] T. Mahmoudi, Y. Wang, Y.-B. Hahn, *ACS Energy Lett.* **2019**, *4*, 235.

[68] X. Gong, L. Guan, Q. Li, Y. Li, T. Zhang, H. Pan, Q. Sun, Y. Shen, C. Grätzel, S. M. Zakeeruddin, M. Grätzel, M. Wang, *Sci. Adv.* **2020**, *6*, eaay5661.

[69] H. Li, L. Tao, F. Huang, Q. Sun, X. Zhao, J. Han, Y. Shen, M. Wang, *ACS Appl. Mater. Interfaces* **2017**, *9*, 38967.

[70] L. Najafi, B. Taheri, B. Martín-García, S. Bellani, D. Di Girolamo, A. Agresti, R. Oropesa-Nuñez, S. Pescetelli, L. Vesce, E. Calabrò, M. Prato, A. E. Del Rio Castillo, A. Di Carlo, F. Bonaccorso, *ACS Nano* **2018**, *12*, 10736.

[71] Z.-E. Shi, S.-H. Liu, C.-H. Tsai, C.-W. Li, C.-P. Chen, Y.-H. Yu, *FlatChem* **2021**, *28*, 100254.

[72] W. Ke, M. G. Kanatzidis, *Nat. Commun.* **2019**, *10*, 965.

[73] T. Mahmoudi, M. Kohan, W.-Y. Rho, Y. Wang, Y. H. Im, Y.-B. Hahn, *Adv. Energy Mater.* **2022**, *12*, 2201977.

[74] T. Liu, Y. Liu, M. Chen, X. Guo, S. Tang, R. Zhang, Z. Xie, J. Wang, A. Gu, S. Lin, N. Wang, *Adv. Funct. Mater.* **2022**, *32*, 2106779.

[75] S. Ameen, M. A. Rub, S. A. Kosa, K. A. Alamry, M. S. Akhtar, H.-S. Shin, H.-K. Seo, A. M. Asiri, M. K. Nazeeruddin, *ChemSusChem* **2016**, *9*, 10.

[76] Z. Hawash, L. K. Ono, Y. Qi, *Adv. Mater. Interfaces* **2018**, *5*, 1700623.

[77] Y. Wang, L. Duan, M. Zhang, Z. Hameiri, X. Liu, Y. Bai, X. Hao, *Sol. RRL* **2022**, *6*, 2200234.

[78] a) M. Wang, H. Wang, W. Li, X. Hu, K. Sun, Z. Zang, *J. Mater. Chem. A* **2019**, *7*, 26421; b) Y.-C. Chin, M. Daboczi, C. Henderson, J. Luke, J.-S. Kim, *ACS Energy Lett.* **2022**, *7*, 560.

[79] a) P. Ru, E. Bi, Y. Zhang, Y. Wang, W. Kong, Y. Sha, W. Tang, P. Zhang, Y. Wu, W. Chen, X. Yang, H. Chen, L. Han, *Adv. Energy Mater.* **2020**, *10*, 1903487; b) E. H. Jung, N. J. Jeon, E. Y. Park, C. S. Moon, T. J. Shin, T.-Y. Yang, J. H. Noh, J. Seo, *Nature* **2019**, *567*, 511.

[80] P. You, G. Tang, J. Cao, D. Shen, T.-W. Ng, Z. Hawash, N. Wang, C.-K. Liu, W. Lu, Q. Tai, Y. Qi, C.-S. Lee, F. Yan, *Light: Sci. Appl.* **2021**, *10*, 68.

[81] Z. Wu, S. Bai, J. Xiang, Z. Yuan, Y. Yang, W. Cui, X. Gao, Z. Liu, Y. Jin, B. Sun, *Nanoscale* **2014**, *6*, 10505.

[82] S.-S. Li, K.-H. Tu, C.-C. Lin, C.-W. Chen, M. Chhowalla, *ACS Nano* **2010**, *4*, 3169.

[83] S. Feng, Y. Yang, M. Li, J. Wang, Z. Cheng, J. Li, G. Ji, G. Yin, F. Song, Z. Wang, J. Li, X. Gao, *ACS Appl. Mater. Interfaces* **2016**, *8*, 14503.

[84] J. Niu, D. Yang, X. Ren, Z. Yang, Y. Liu, X. Zhu, W. Zhao, S. Liu, *Org. Electron.* **2017**, *48*, 165.

[85] C. K. Chua, M. Pumera, *Chem. Soc. Rev.* **2014**, *43*, 291.

[86] J.-S. Yeo, R. Kang, S. Lee, Y.-J. Jeon, N. Myoung, C.-L. Lee, D.-Y. Kim, J.-M. Yun, Y.-H. Seo, S.-S. Kim, S.-I. Na, *Nano Energy* **2015**, *12*, 96.

[87] L. Sygellou, G. Paterakis, C. Galiotis, D. Tasis, *J. Phys. Chem. C* **2016**, *120*, 281.

[88] A. L. Palma, L. Cinà, S. Pescetelli, A. Agresti, M. Raggio, R. Paolesse, F. Bonaccorso, A. Di Carlo, *Nano Energy* **2016**, *22*, 349.

[89] J.-J. Park, M. Lee, Y. Kim, D.-Y. Kim, *Sol. RRL* **2021**, *5*, 2100087.

[90] S. Suragtkhuu, O. Tserendavag, U. Vandandoo, A. S. R. Bati, M. Bat-Erdene, J. G. Shapter, M. Batmunkh, S. Davaasambuu, *RSC Adv.* **2020**, *10*, 9133.

[91] X. Wang, X. Yu, J. Song, W. Huang, Y. Xiang, X. Dai, H. Zhang, *Chem. Eng. J.* **2021**, *406*, 126876.

[92] S. Liu, J. Lyu, D. Zhou, X. Zhuang, Z. Shi, R. Sun, L. Liu, Y. Wu, B. Liu, D. Liu, H. Song, *Adv. Funct. Mater.* **2022**, *32*, 2112647.

[93] M. Zhang, M. Ye, W. Wang, C. Ma, S. Wang, Q. Liu, T. Lian, J. Huang, Z. Lin, *Adv. Mater.* **2020**, *32*, 2000999.

[94] J. He, F. Zhang, Y. Xiang, J. Lian, X. Wang, Y. Zhang, X. Peng, P. Zeng, J. Qu, J. Song, *J. Power Sources* **2019**, *435*, 226819.

[95] M. Bat-Erdene, G. Xu, M. Batmunkh, A. S. R. Bati, J. J. White, M. J. Nine, D. Losic, Y. Chen, Y. Wang, T. Ma, J. G. Shapter, *J. Mater. Chem. A* **2020**, *8*, 4735.

[96] A. Y. Goharrizi, P. S. Parsa, *2022 30th International Conference on Electrical Engineering (ICEE)*, ICEE, Tehran, Iran **2022**, https://doi.org/10.1109/ICEE55646.2022.9827319905.

[97] a) M. Batmunkh, C. J. Shearer, M. J. Biggs, J. G. Shapter, *J. Mater. Chem. A* **2015**, *3*, 9020; b) R. Chen, W. Zhang, X. Guan, H. Raza, S. Zhang, Y. Zhang, P. A. Troshin, S. A. Kuklin, Z. Liu, W. Chen, *Adv. Funct. Mater.* **2022**, *32*, 2200651.

[98] A. Mei, X. Li, L. Liu, Z. Ku, T. Liu, Y. Rong, M. Xu, M. Hu, J. Chen, Y. Yang, M. Grätzel, H. Han, *Science* **2014**, *345*, 295.

[99] K. Yan, Z. Wei, J. Li, H. Chen, Y. Yi, X. Zheng, X. Long, Z. Wang, J. Wang, J. Xu, S. Yang, *Small* **2015**, *11*, 2269.

[100] M. Guo, C. Wei, C. Liu, K. Zhang, H. Su, K. Xie, P. Zhai, J. Zhang, L. Liu, *Mater. Des.* **2021**, *209*, 109972.

[101] P. You, Z. Liu, Q. Tai, S. Liu, F. Yan, *Adv. Mater.* **2015**, *27*, 3632.

[102] C. Zhang, S. Wang, H. Zhang, Y. Feng, W. Tian, Y. Yan, J. Bian, Y. Wang, S. Jin, S. M. Zakeeruddin, M. Grätzel, Y. Shi, *Energy Environ. Sci.* **2019**, *12*, 3585.

[103] C. Zhang, S. Liang, W. Liu, F. T. Eickemeyer, X. Cai, K. Zhou, J. Bian, H. Zhu, C. Zhu, N. Wang, Z. Wang, J. Zhang, Y. Wang, J. Hu, H. Ma, C. Xin, S. M. Zakeeruddin, M. Grätzel, Y. Shi, *Nat. Energy* **2021**, *6*, 1154.

[104] Z. Hu, Y. Zhao, W. Zou, Q. Lu, J. Liao, F. Li, M. Shang, L. Lin, Z. Liu, *Adv. Funct. Mater.* **2022**, *32*, 2203179.

[105] M. Batmunkh, A. Shrestha, G. Gao, L. Yu, J. Zhao, M. J. Biggs, C. J. Shearer, J. G. Shapter, *Sol. RRL* **2017**, *1*, 1700011.

[106] Y. Zhu, S. Jia, J. Zheng, Y. Lin, Y. Wu, J. Wang, *J. Mater. Chem. C* **2018**, *6*, 3097.

[107] Z. Liu, J. Li, Z.-H. Sun, G. Tai, S.-P. Lau, F. Yan, *ACS Nano* **2012**, *6*, 810.

[108] M. Batmunkh, Y. L. Zhong, H. Zhao, *Adv. Mater.* **2020**, *32*, 2000631.

[109] J. Shan, C. Ye, Y. Jiang, M. Jaroniec, Y. Zheng, S.-Z. Qiao, *Sci. Adv.* **2022**, *8*, eabo0762.

Selengesuren Suragtkhuu is currently a Ph.D. candidate in the School of Environment and Science, and Queensland Micro- and Nanotechnology Centre at Griffith University. She completed her "Master of Science" in 2022, and a combined degree of "Bachelor of Science" and "Bachelor of Engineering" in 2020 at the National University of Mongolia. She represented Mongolia for the International Chemistry Olympiad (ICHO) twice, in Vietnam 2014 and in Azerbaijan 2015. Her research interests focus on 2D materials, photovoltaic (perovskite solar cells) and catalysis.

Suvdanchimeg Sunderiya is currently an undergraduate student in the School of Arts and Sciences at the National University of Mongolia, majoring in chemistry. She participated in the 49th and 50th International Chemistry Olympiad (ICHO) in Thailand (2017) and Czech Republic (2018); and won two bronze medals. Her current research focuses on designing functional 2D layered materials as efficient catalysts for electrochemical water splitting.

Purevlkham Myagmarsereejid is pursuing her Ph.D. degree from the School of Environment and Science, and Queensland Micro- and Nanotechnology Centre at Griffith University. She received her M.Sc. and B.Sc. degrees in chemistry from the National University of Mongolia, in 2014 and 2011, respectively. She also worked as a research assistant at the Institute of Chemistry and Chemical Technology in the Mongolian Academy of Sciences from 2015 to 2016. Her research interests include the production of 2D materials for antimony sulfide and perovskite solar cells.

Solongo Purevdorj graduated with "Bachelor of Science" degree from the School of Chemistry and Chemical Engineering at the National University of Mongolia, Mongolia in 2011. She then received her "Master of Science" degree in electrochemistry from the National University of Mongolia in 2013. After gaining valuable industry experience as a chemical analyst (from 2014), she joined the Department of Chemistry in the National University of Mongolia, as a research assistant in 2021. She expects to join Griffith University as a Ph.D. candidate from mid-2023. Her current research interests are 2D materials for perovskite solar cells and their role and stability.

Abdulaziz S. R. Bati obtained his Ph.D. from the Australian Institute for Bioengineering and Nanotechnology (AIBN) at the University of Queensland (UQ) in 2021. He is currently a KAUST Ibn Rushd Postdoctoral Fellow hosted by the Centre for Organic Photonics and Electronics (COPE) at UQ. Prior to this, he was a Postdoctoral Research Fellow at COPE. His research interests mainly focus on functional nanomaterials and their applications in third-generation photovoltaics, particularly perovskite solar cells.

ADVANCED
SCIENCE NEWS

www.advancedsciencenews.com

ADVANCED
ENERGY
MATERIALS

www.advenergymat.de

Bujinlkham Bold is currently a CEO of Nano group which consists of real estate, FMCG, and energy companies in Mongolia. The group is committed to developing and contributing to the country through its pursuit of innovation. She completed her Master degree in Nanotechnology at the Flinders University of South Australia in 2014. She has Bachelor degrees in Business and Science from the National University of Mongolia. She has strong interests in supporting innovative research in the areas of nanomaterials and renewable energy technologies.

Yu Lin Zhong is currently an associate professor and ARC Future Fellow at Griffith University School of Environment and Science, and Queensland Micro- and Nanotechnology Centre. He completed his Ph.D. in Chemistry at National University of Singapore and did his post-doctoral training at Princeton University (2009) and Massachusetts Institute of Technology (2011). Thereafter, he worked as a Research Scientist at Institute of Bioengineering and Nanotechnology, A*STAR Singapore, (2012) and an ARC DECRA Fellow at Monash University (2013). His research group interests include electrochemical production of 2D nanomaterials and 3D printing of energy storage and wearable devices.

Sarangerel Davaasambuu is currently a professor in the Department of Chemistry, Division of Natural Sciences, School of Arts and Sciences at the National University of Mongolia. She obtained her Ph.D. degree in Environmental Sciences from the Tohoku University of Japan in 2007. Her group conducts research on the kinetic and thermodynamic interpretation of adsorption and electrocoagulation, chemical and biological leaching, and electrocatalytic activity of 2D materials.

Munkhbayar Batmunkh is currently a lecturer and ARC DECRA Fellow in the School of Environment and Science, and Queensland Micro- and Nanotechnology Centre at Griffith University. He completed his Ph.D. in chemical engineering at the University of Adelaide (Australia) in 2017. He received his M.E. and B.Sc. degrees in 2012 and 2010 from Gyeongsang National University (South Korea) and National University of Mongolia (Mongolia), respectively. He currently leads an active independent research group at Griffith University working on the development of functional nanomaterials, solar cells, catalysis, and photovoltaic-integrated new technologies.